MOLECULAR AND CELLULAR BIOLOGY, July 2004, p. 6379–6392 Vol. 24, No. 14
0270-7306/04/$08.00+0 DOI: 10.1128/MCB.24.14.6379–6392.2004

The Fission Yeast Nup107-120 Complex Functionally Interacts with the Small GTPase Ran/Spi1 and Is Required for mRNA Export, Nuclear Pore Distribution, and Proper Cell Division

Siau Wei Baï,[1] Jacques Rouquette,[2]† Makoto Umeda,[3]† Wolfgang Faigle,[4] Damarys Loew,[4] Shelley Sazer,[3] and Valérie Doye[1]*

UMR 144 CNRS[1] and Laboratoire de Spectrométrie de Masse Protéomique,[4] Institut Curie, 75248 Paris Cedex 05, and Laboratoire de Biologie Moléculaire Eucaryote (UMR 5099-CNRS), Université Paul Sabatier, 31062 Toulouse Cedex,[2] France, and Department of Biochemistry and Molecular Biology, Baylor College of Medicine, Houston, Texas 77030[3]

Received 19 November 2003/Returned for modification 26 January 2004/Accepted 26 April 2004

We have characterized *Schizosaccharomyces pombe* open reading frames encoding potential orthologues of constituents of the evolutionarily conserved *Saccharomyces cerevisiae* Nup84 vertebrate Nup107-160 nuclear pore subcomplex, namely Nup133a, Nup133b, Nup120, Nup107, Nup85, and Seh1. In spite of rather weak sequence conservation, in vivo analyses demonstrated that these *S. pombe* proteins are localized at the nuclear envelope. Biochemical data confirmed the organization of these nucleoporins within conserved complexes. Although examination of the *S. cerevisiae* and *S. pombe* deletion mutants revealed different viability phenotypes, functional studies indicated that the involvement of this complex in nuclear pore distribution and mRNA export has been conserved between these highly divergent yeasts. Unexpectedly, microscopic analyses of some of the *S. pombe* mutants revealed cell division defects at the restrictive temperature (abnormal septa and mitotic spindles and chromosome missegregation) that were reminiscent of defects occurring in several *S. pombe* GTPase Ran (Ran^{Sp})/Spi1 cycle mutants. Furthermore, deletion of *nup120* moderately altered the nuclear location of Ran^{Sp}/Spi1, whereas overexpression of a nonfunctional Ran^{Sp}/Spi1-GFP allele was specifically toxic in the Δ*nup120* and Δ*nup133b* mutant strains, indicating a functional and genetic link between constituents of the *S. pombe* Nup107-120 complex and of the Ran^{Sp}/Spi1 pathway.

Traffic of macromolecules between the nuclear and cytoplasmic compartments, which is fundamental in eukaryotic cells, occurs through the nuclear pore complexes (NPCs), which are macromolecular assemblies embedded in the nuclear envelope (NE). Active nucleocytoplasmic transport of most macromolecules involves a series of interactions among nuclear pore proteins (nucleoporins), soluble transport factors (karyopherins), and cargos that are modulated by the small Ras-like GTPase Ran (reviewed in references 39 and 55). In contrast, export of most spliced mRNA appears to be independent of the Ran-importin β machinery (12, 33). In addition to regulating nuclear transport, Ran plays additional and independent roles in many other cellular processes, including microtubule dynamics and mitotic-spindle formation, regulation of cell cycle progression, and postmitotic NE and NPC assembly (3, 15, 28, 31, 35, 52, 54, 69).

In recent years, extensive progress has been made in the identification and characterization of all NPC components, using proteomic and genomic approaches. *Saccharomyces cerevisiae* and vertebrate NPCs are composed of roughly 30 nucleoporins, of which about two-thirds have been conserved during evolution (14, 51). While the molecular dissection of NPCs is nearly complete in these organisms, only a few nucleoporins have been definitively identified so far in fission yeast. As *Schizosaccharomyces pombe* and *S. cerevisiae* are evolutionary distant, interspecies comparisons should allow the dissection of conserved functions with more precision, thereby improving our understanding of NPC function during evolution. Indeed, comparisons of a few *S. cerevisiae* and *S. pombe* nucleoporin orthologues have revealed unexpected functional divergences (71, 73).

In this paper, therefore, we have undertaken the functional analysis of the *S. pombe* orthologues of *S. cerevisiae* Nup84 (ScNup84)/vertebrate Nup107-160 complex constituents. In *S. cerevisiae*, this complex is composed of Nup84, Nup85, Nup120, Nup145-C, Seh1, Sec13, and Nup133 (2, 38, 58, 59, 65). In this organism, single mutations in members of the Nup84 complex are not lethal (although double mutations cause synthetic lethality), but most of them lead to a temperature-sensitive growth defect, to nuclear poly(A)$^+$ RNA accumulation at the restrictive temperature, and to NPC clustering at all temperatures. The vertebrate counterpart of the ScNup84 complex, named the Nup107-160 complex (7, 67), has also been demonstrated to be involved in mRNA export and NPC assembly (9, 28, 67, 68). Our study revealed major differences in the viability phenotypes of the corresponding *S. cerevisiae* and *S. pombe* deletion mutants and some differences in the behaviors of these nucleoporins during biochemical fractionation. Functional studies also suggested that the involvement of the complex in NPC distribution and poly(A)$^+$ RNA export has been at least partly conserved between these highly divergent yeasts. However, our study also revealed cell division defects in some of these *S. pombe* mutant strains. The involve-

* Corresponding author. Mailing address: UMR 144 CNRS-Institut Curie, 26 Rue d'Ulm, 75248 Paris Cedex 05, France. Phone: (33) 1 42 34 64 10. Fax: (33) 1 42 34 64 21. E-mail: vdoye@curie.fr.
† J.R. and M.U. contributed equally to this work.

TABLE 1. Fission yeast strains used in this study

Strain		Genotype	Source
SP826	h^+/h^+	*ade6-210/ade6-216 ura4-D18/ura4-D18 leu1-32/leu1-32*	D. Beach
FC420	h^+	*ade6-216 ura4-D18 leu1-32*	F. Chang
FC418	h^-	*ade6-210 ura4-D18 leu1-32*	F. Chang
SPV21	h^+/h^+	*nup107*$^+$/Δ*nup107*::*kanMX ade6-210/ade6-216 ura4-D18/ura4-D18 leu1-32/leu1-32*	This study
SPV25	h^+/h^+	*nup133a*$^+$/Δ*nup133a*::*kanMX ade6-210/ade6-216 ura4-D18/ura4-D18 leu1-32/leu1-32*	This study
SPV94	h^+/h^+	*nup85*$^+$/Δ*nup85*::*kanMX ade6-210/ade6-216 ura4-D18/ura4-D18 leu1-32/leu1-32*	This study
SPV97	h^+/h^+	*nup120*$^+$/Δ*nup120*::*kanMX ade6-210/ade6-216 ura4-D18/ura4-D18 leu1-32/leu1-32*	This study
SPV560	h^+/h^+	*seh1*$^+$/Δ*seh1*::*kanMX ade6-210/ade6-216 ura4-D18/ura4-D18 leu1-32/leu1-32*	This study
SPV34	h^+	Δ*nup133a*::*kanMX ade6-210 ura4-D18 leu1-32*	This study
SPV53	h^-	Δ*nup133b*::*kanMX ade6-210 ura4-D18 leu1-32*	This study
SPV56	h^-	Δ*nup133a*::*kanMX nup133b*Δ::*kan*^{r} *ade6-216 ura4-D18 leu1-32*	This study
SPV113	h^+	Δ*nup120*::*kanMX ade6-210 ura4-D18 leu1-32*	This study
SPV561	h^+	Δ*seh1*::*kanMX ade6-210 ura4-D18 leu1-32*	This study
SPV33	h^+	*nup107*-GFP(S65T)::*kanMX ade6-216 ura4-D18 leu1-32*	V. Doye
SPV477	h^-	*kanMX-P3nmt1*-GFP(S65T)-*nup85 ade6-210 ura4-D18 leu1-32*	This study
SPV639	h^+	*kanMX-P3nmtl*-GFP(S65T)-*seh1 ade6*$^-$ *ura4-D18 leu1-32*	This study
SPV76	$h^?$	*nup107*-GFP(S65T)::*kanMX* Δ*nup133a*::*kanMX ade6*$^-$ *ura4-D18 leu1-32*	This study
SPV72	$h^?$	*nup107*-GFP(S65T)::*kanMX* Δ*nup133b*::*kanMX ade6*$^-$ *ura4-D18 leu1-32*	This study
SPV584	$h^?$	*nup107*-GFP(S65T)::*kanMX* Δ*nup120*::*kanMX* + pREP4X-HA_3-Nup120 *ade6*$^-$ *leu1-32*	This study
SPV574	$h^?$	*kanMX-P3nmt1*-GFP(S65T)-*nup85* Δ*nup133a*::*kanMX ade6*$^-$ *ura4-D18 leu1-32*	This study
SPV572	$h^?$	*kanMX-P3nmt1*-GFP(S65T)-*nup85* Δ*nup133b*::*kanMX ade6*$^-$ *ura4-D18 leu1-32*	This study
SPV583	$h^?$	*kanMX-P3nmt1*-GFP(S65T)-*nup85* Δ*nup120*::*kanMX* + pREP4X-HA_3-Nup120 *ade6*$^-$ *leu1-32*	This study
SPV697	$h^?$	*kanMX-P3nmt1*-GFP(S65T)-*seh1* Δ*nup133a*::*kanMX ade6*$^-$ *ura4-D18 leu1-32*	This study
SPV701	$h^?$	*kanMX-P3nmt1*-GFP(S65T)-*seh1* Δ*nup133b*::*kanMX ade6*$^-$ *ura4-D18 leu1-32*	This study
Δnup184	h^+	Δ*nup184*::*ura4*$^+$ *ade6*$^-$ *leu1-32*	R. Dhar
Δmad2	h^-	Δ*mad2*::*ura4*$^+$ *ade6-210 ura4-D18 leu1-32*	S. Sazer
Δmph1	h^-	Δ*mph1*::*ura4*$^+$ *ade6-216 ura4-D18 leu1-32*	S. Sazer
SPV526	$h^?$	Δ*nup120*::*kanMX* Δ*mad2*::*ura4 ade6*$^-$ *leu1-32 ura4-D18*	This study
SPV531	$h^?$	Δ*nup120*::*kanMX* Δ*mph1*::*ura4 ade6*$^-$ *leu1-32 ura4-D18*	This study
YP10.22a	h^+	Ch^{16} (*ade6-216*); *ade6-210 ura4-D6 leu1-32*	M. Yanagida
SPV323	$h^?$	Δ*nup120*::*kanMX* + pREP4X-HA_3-Nup120 Ch^{16} (*ade6-216*) *ade6-210 leu1-32*	This study
SPV327	$h^?$	Δ*nup120*::*kanMX* + pREP4X-HA_3-Nup120 *ade6-210 leu1-32*	This study
NC102+p(nuc2$^+$)	h^-	*nuc2-663* + pLEU2-(*nuc2*$^+$) *leu1-32*	M. Yanagida
MA217	h^+	*nuf2*-CFP::*kanMX ura4-D18 leu1-32 his2*$^-$	T. Toda
SPV830	$h^?$	*kanMX-P3nmt1*-GFP(S65T)-*nup85 nuc2-663 Nuf2-CFP*::*kanMX ura4-D18 leu1-32*	This study

ment of the *S. pombe* Ran (Ran^{Sp})/Spi1 pathway with respect to the various phenotypes associated with perturbations of the functions of the *S. pombe* Nup107-120 (SpNup107-120) complex is discussed.

MATERIALS AND METHODS

BLAST searches at the Sanger Center *S. pombe* server were used to identify open reading frames (ORFs) encoding proteins similar to *S. cerevisiae* or murine nucleoporins. Sequence comparisons were performed using ClustalW (http://clustalw.genome.ad.jp/).

***S. pombe* strains, media, and genetic techniques.** The strains used in this study are listed in Table 1. Standard cell culture procedures and media were used (44). The strains were grown in rich nonselective yeast extract medium (YE5S) or in synthetic Edinburgh minimal medium (EMM), appropriately supplemented. Sporulation was performed in malt extract medium at 25 or 30°C. Yeast transformation was achieved by the lithium acetate-dimethyl sulfoxide method (6). The thiamine-regulable *nmt1* promoter, in expression vector pREP (43), was repressed by the addition of 5 μg of thiamine/ml of EMM. Phloxine B solution (Bio 101 Systems, Qbiogen, Carlsbad, Calif.) was used at 0.25 ml/liter. Sensitivity to thiabendazole (TBZ) (Sigma) was monitored at 23°C by 10-fold serial-dilution colony spotting on YE5S plates containing the microtubule drug at the appropriate concentrations.

***S. pombe* disruption and genomic green fluorescent protein (GFP)-tagging strategy for *nup107*, *nup85*, *nup120*, *nup133a*, *nup133b*, and *seh1*.** One-step gene disruption (6) was carried out in an h^+/h^+ diploid strain by homologous integration of a PCR fragment corresponding to the KanMX6 module (conferring G418 resistance) in the *nupX* ORFs of interest (*nup107*, *nup85*, *nup120*, *nup133a*, *nup133b*, or *seh1*). YE5S containing 100 or 200 mg of G418/ml was used for selecting $G418^R$ cells, and correct gene targeting was confirmed by PCR analysis. After induction of meiosis, h^+/h^{90} Δ*nupX*::*kanMX6*/*nupX*$^+$ sporulating colonies were identified by iodine exposure, and tetrads were microdissected. N-terminal tagging of Nup85 and Seh1 expressed under the control of the *nmt1* promoter in their chromosomal locations was accomplished by an analogous method (6) using the pFA6a-kanMX6-P3nmt1-GFP vector.

Plasmids. An XhoI-SmaI fragment corresponding to the *nup133a* ORF was first PCR amplified from genomic DNA using the Sp133a-Xho1F and Sp133a-SmaIR oligonucleotides (sequences of all oligonucleotides used are available upon request) and cloned into pBluescript. The XhoI-SmaI fragment was then subcloned into the pREP3 vector (43), in which the GFPmut2 ORF (13) had been previously inserted as an XhoI/SalI fragment, to generate pREP3-GFP(mut2)-Nup133a and into the pSLF173 vector (21) digested with SalI and SmaI to generate pREP4X-HA_3-Nup133a.

A cDNA encoding the N-terminal domain of Nup133b and obtained by reverse transcription-PCR and a DNA fragment corresponding to the C-terminal domain of Nup133b, PCR amplified from genomic DNA, were ligated in pASΔΔCyHA to generate pASΔΔCyHA-Nup133b (7). For the construction of pREP4X-GFP-Nup133b or pREP4X-HA_3-Nup133b, an NcoI-blunt-ended/SmaI fragment of pASΔΔCyHA-Nup133b was cloned at the SmaI site of pSGP573 (http://pingu.salk.edu/~forsburg/vectors.html) or pSLF173, respectively.

The *nup120* ORF was PCR amplified from genomic DNA and was cloned in the pSLF173 vector. To construct the pREP4X-GFP-Nup120 plasmid, the NotI-SmaI insert of pREP4X-HA_3-Nup120 was subcloned into pSGP573.

The NLS-GFP-LacZ-containing fragment from the *S. cerevisiae* plasmid pPS817 (36) was subcloned into pREP4X (20). Plasmids pREP82X-GFP-*nsp1* (74), pREP3X-Spi1 (42), and pREP41X-Spi1-GFP (63) were previously described.

Immunoprecipitation experiments. *S. pombe* Δ*nupX*/GFP-tagged NupY strains expressing HA_3-tagged *nupX* (*nupX* is *nup133a*, *nup133b*, or *nup120*; *nupY* is *nup85*, *nup107*, or *seh1*) were constructed by genetic crossing. The strains were grown at 30°C to log phase in supplemented EMM in the presence of thiamine to avoid overexpression of the tagged nucleoporins. For whole-cell lysate prep-

TABLE 2. Amino acid sequence comparison of the *S. pombe*, *S. cerevisiae*, and human nucleoporins of the Nup107-120 complex[a]

S. pombe		*S. cerevisiae*		*H. sapiens*		% Identity/% similarity[b]			
Name (ORF)	Mass	Name	Mass	Name	Mass	Sc/Sp	Hs/Sp	Hs/Sc	Sp/Sp
Nup107 (SPBC582.11c)	91	Nup84	84	Nup107	107	21/45	24/46	18/42	
Nup85 (SPBC17G9.04c)	78	Nup85	85	Nup85/Nup75	75	17/42	15/35	14/36	
Nup120 (SPBC3B9.16c)	130	Nup120	120	Nup120/Nup160	160	14/35	14/33	14/35	
Nup133a (SPBP35G2.06c)	131	Nup133	133	Nup133	129	16/38	12/30	11/32	19/42
Nup133b (SPAC1805.04)	132					18/40	10/28		
Seh1 (SPAC15F9.02)	38	Seh1	39	Seh1	40	41/66	39/62	33/56	

[a] The name and predicted mass (in kilodaltons) of each nucleoporin are indicated. To avoid additional nomenclature, these proteins have been named according to the first homologous nucleoporin identified. The *S. pombe* GeneDB systematic names are also specified (http://www.genedb.org/genedb/pombe/index.jsp). To fit the *S. pombe* gene nomenclature, SpNup133a and SpNup133b also appear as Nup131 and Nup132 in the *S. pombe* GeneDB.

[b] Percentages of identity and similarity among *S. pombe* (Sp), *S. cerevisiae* (Sc), and *Homo sapiens* (Hs) nucleoporins were calculated using ClustalW (http://clustalw.genome.ad.jp/). Alignments of *S. cerevisiae*, *S. pombe*, and human Nup107, Nup85, Seh1 (unpublished data), Nup133, and Nup120/160 (7) indicate that the similarity is spread over the entire sequence and does not allow the identification of functional domains within these nucleoporins.

aration, ~10^9 cells were washed in stop buffer and resuspended in immunoprecipitation buffer as previously described (60), with the following changes: Triton was replaced by 1% NP-40, and aprotinin and pepstatin were replaced by a protease inhibitor cocktail (Roche). The cells were then broken with glass beads in a Fastprep (Bio 101 Systems) and spun, and the supernatants were recovered. Protein G-Sepharose beads (Amersham Biosciences) were loaded with anti-GFP antibodies (Roche) in A buffer (50 mM HEPES, pH 7.5, 100 mM NaCl, 1 mM EDTA) at 4°C for 2 h. After four washes in A buffer, the beads were incubated with the extracts at 4°C for 3 h, washed five times in A buffer supplemented with 1% NP-40 and then once in A buffer, and resuspended in loading buffer. The resulting samples were analyzed by sodium dodecyl sulfate-polyacrylamide gel electrophoresis followed by Western blotting using anti-GFP or -HA (12CA5) antibodies. The antibodies were detected using horseradish-peroxidase-conjugated goat anti-mouse secondary antibodies. Immunoblots were visualized using enhanced-chemiluminescence reagents (Pierce).

For mass spectrometry analysis, after coloration with colloidal Coomassie blue (G250; Bio-Rad), the protein spots were excised from the gel, reduced using dithiothreitol, and alkylated using iodoacetamide. The proteins were subjected to digestion with trypsin (Sigma) following the protocol of Shevchenko et al. modified by overnight digestion at 30°C (57). The extracted peptides were analyzed by matrix-assisted laser desorption-ionization–time of flight mass spectrometry (Voyager-DETM PRO; Applied Biosystems). Peptide masses obtained by this analysis were used to search the National Center for Biotechnology Information database to identify the full-length proteins.

Fluorescence and electron microscopy. Fluorescence in situ hybridization (FISH) for poly(A)$^+$ RNA was performed as described by Brown et al. (10), with the following modifications: spheroplasts were obtained by digestion with 0.1 mg of Zymolyase-100T (Seikagaku)/ml in PEM buffer {50 mM PIPES [piperazine-*N*,*N*′-bis(2-ethanesulfonic acid)], pH 6.9, 0.5 mM EGTA, 0.5 mM $MgSO_4$} plus 1 M sorbitol, and the 50-nucleotide oligo(dT) probe was directly coupled to Cy3 (Amersham Pharmacia Biotech). To detect the distribution of the pre-60S ribosomal particles, FISH was also performed using a probe complementary to the 25S rRNA, conserved from *S. cerevisiae* to *S. pombe* (5′ CCCGTTCCCTTGGC TGTGGTTTCGCTAGAT*A 3′, where the asterisk represents amino-purified nucleotides coupled with Cy3) (26).

Stainings of the cell walls and septa and the nuclei of formaldehyde-fixed cells were carried out using calcofluor (2 μg/ml; Sigma) and DAPI (4′,6′-diamidino-2-phenylindole; 1 μg/ml) (48). Tubulin immunofluorescence of formaldehyde-fixed cells was performed as described previously (48), using a TAT1 monoclonal antibody (72) together (when indicated) with an anti-Mid1 rabbit antibody (48). Spi1p was localized using affinity-purified rabbit anti-Spi1p antibody (41), and NPCs were visualized using mAb414 (BAbCO) as previously described (16).

Images of fixed cells and of live cells expressing GFP- or cyan fluorescent protein (CFP)-tagged proteins were acquired with an upright motorized widefield microscope (DMRA2; Leica), using an oil immersion objective (100× PL APO HCX; 1.4 numerical aperture) and a high-sensitivity cooled interlined charge-coupled device camera (CoolSnap HQ; Roper). For some observations, stacks were acquired using a piezo-electric motor (LVDT; Physik Instrument) mounted underneath the objective lens. The whole system was controlled with Metamorph 5 software (Universal Imaging Corp.). Z sections of DAPI signals (see Fig. 7) were converted into single two-dimensional images by taking the maximum signal at each pixel position in the images. The length of the mitotic spindle (see Fig. 8) was determined based on a two-dimensional projection of Z sections, and used to determine approximate classes as follows: premetaphase, <2 μm; metaphase, 2 to 3 μm; early anaphase, 3 to 5 μm; late anaphase, >5 μm. For deconvolution (see Fig. 5A and 9D), image stacks were acquired without camera binning, with a plane spacing of 0.2 μm, leading to a voxel size of 64.5 by 64.5 by 200 nm^3. Deconvolution was performed by the three-dimensional deconvolution module from Metamorph (Universal Imaging Corp.), using the fast iterative constrained PSF-based algorithm. Images in Fig. 10A were obtained with a Zeiss Axioskop microscope, and digitized images were captured with a DVC 1300 charge-coupled device camera and QED software.

Thin-section electron microscopy was performed as described previously (49), using cells freshly grown overnight on YE5S plates at semipermissive temperature (30°C).

Fluorescence-activated cell-sorting (FACS) analysis. The DNA content was analyzed as described previously (62), using a Becton Dickinson FACSCalibur with the following modifications: buffer A was replaced by 50 mM sodium citrate, pH 7.5, and RNase A was added to a final concentration of 0.5 mg/ml and incubated at 37°C for 3 h. Propidium iodide was then added to a final concentration of 5 μg/ml.

Chromosome loss assays. The YP10.22 strain, containing a 550-kb minichromosome (47), was crossed with a haploid Δ*nup120* strain carrying the pREP4X-HA_3-Nup120 plasmid (*ura4*$^+$ marker). After dissection, a Δ*nup120* strain carrying pREP4X-HA_3-Nup120 and containing or lacking the minichromosome were isolated and then spotted at 23°C onto EMM plates supplemented with 1 mg of 5-fluoroorotic acid (5-FOA)/ml and 50 mg of uracil/liter to select for cells able to lose the *ura4*$^+$-containing plasmid. Chromosome loss was also monitored in *ade6-M210*/*ade6-M216* h^+/h^+ diploid strains. For scoring Ade$^-$ phenotypes, cells from 10 small colonies were plated after dilution on yeast extract medium and cultured at 30 or 36°C for ~3 days. The percentage of pink colonies (chromosome loss event) was determined, taking the average of four independent experiments.

RESULTS

The Nup107 complex is conserved in fission yeast. By searching public databases, several *S. pombe* ORFs encoding proteins with moderate sequence similarity to constituents of the ScNup84 and the human Nup107-160 complexes were identified. They included putative homologues of *S. cerevisiae* Nup133 (designated Nup133a and Nup133b), Nup120, Nup84, Nup85, Nup145-C, and Seh1 (Table 2) (7, 14, 66, 67). Because of the low levels of sequence similarity between these *S. pombe* proteins and their *S. cerevisiae* and human counterparts (Table 2), we first asked whether these proteins were bona fide nucleoporins. It was previously reported that Nup107-GFP was localized at the NE (66) (Fig. 1). Similarly, in vivo analysis of GFP-tagged Nup85, Seh1, Nup120, Nup133a, and Nup133b revealed punctate rim-like staining around the nucleus, which is typical of NPC localization (Fig. 1).

To determine whether the organization of these nucleoporins in an NPC-subcomplex has been conserved in *S. pombe*,

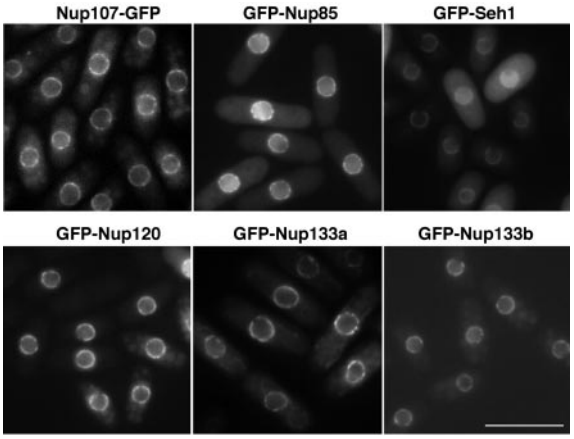

FIG. 1. In vivo localization of GFP-tagged Nup107, Nup85, Seh1, Nup120, Nup133a, and Nup133b in *S. pombe*. Nup107-GFP, GFP-Nup85, and GFP-Seh1 strains were grown in YE5S medium. Δ*nup120*, Δ*nup133a*, and Δ*nup133b* strains expressing GFP-Nup120, GFP-Nup133a and GFP-Nup133b fusion proteins, respectively, were first grown in appropriately supplemented EMM containing thiamine and then shifted overnight to EMM without thiamine. The distribution of the various GFP fusions was observed in live cells. All the fusion proteins localized to the nuclear periphery in a ring-like staining pattern characteristic of nucleoporins. Note that under these growth conditions, the level of the nucleoporins expressed under the control of the *nmt1* promoter is similar to that of Nup107 expressed under the control of its own promoter. Bar, 10 μm.

immunoprecipitation experiments were performed using anti-GFP antibodies on total extracts from *S. pombe* cells expressing Nup107-GFP, GFP-Nup85, GFP-Seh1, or no GFP fusion in strains with *nup133a*, *nup133b*, or *nup120* deleted and complemented by plasmids encoding the corresponding HA-tagged nucleoporins (Table 1). As shown in Fig. 2A, this study revealed that Nup107-GFP efficiently coprecipitated with HA-Nup133a and HA-Nup133b, confirming previous results based on two-hybrid interactions (7), but did not significantly interact with HA-Nup120. Conversely, GFP-Nup85 and GFP-Seh1 efficiently copurified with HA-Nup120 but not with HA-Nup133a or with HA-Nup133b.

Silver and colloidal-blue staining of the GFP-Nup85, GFP-Seh1, and Nup107-GFP precipitates revealed distinct bands that were not present in the control samples (Fig. 2B). Mass spectrometry analysis of some of these bands identified the ~75-kDa polypeptide present solely in the GFP-Seh1 purified fraction as Nup85. The ~110-kDa polypeptide, reproducibly detected in both the GFP-Nup85 and GFP-Seh1 fractions, was identified as the C-terminal domain of an *S. pombe* nucleoporin similar to *S. cerevisiae* Nup145 and mammalian Nup98/96 and designated Nup189 in fission yeast (61). Nup189 was previously shown to be cleaved in vivo, most likely by autoproteolysis, as demonstrated in *S. cerevisiae* and mammals (19, 64), leading to a 95-kDa N-terminal product that interacted with Ned1 in a two-hybrid screen (61). In contrast, the protein identified in our complex corresponds to the *S. pombe* orthologue of ScNup145-C.

Therefore, there are two stable subcomplexes in *S. pombe*, one consisting of Nup120, Nup85, Seh1, and Nup145-C and another comprising Nup107 associated with Nup133a and/or Nup133b (Fig. 2C). Our results thus corroborate the structural model proposed for the *S. cerevisiae* Nup84 complex (38) (Fig. 2C). However, unlike in *S. cerevisiae* or human cells, we were not able to demonstrate a stable interaction between Nup107 or Nup133 and the Nup120-containing subcomplex under the biochemical fractionation employed here. Conversely,

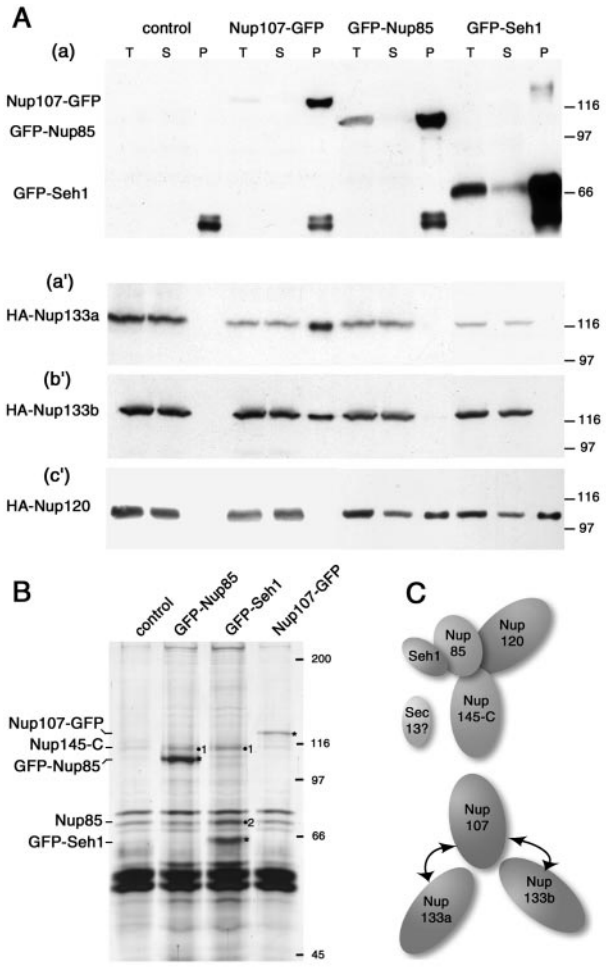

FIG. 2. The *S. pombe* Nup107-120 NPC subcomplex biochemically purifies as two distinct entities. (A) Western blot analysis of immunoprecipitation experiments performed on *S. pombe* whole-cell lysates using an anti-GFP antibody. *S. pombe* strains expressing an HA-Nup133a, -Nup133b, or -Nup120 fusion in a Δ*nup133a*, Δ*nup133b*, or Δ*nup120* background, respectively, and either no GFP fusion or a GFP-tagged nucleoporin (Nup107-GFP, GFP-Nup85, or GFP-Seh1) were grown at 30°C to log phase in supplemented liquid EMM in the presence of thiamine. Immunoprecipitation experiments were performed on these 12 different *S. pombe* whole-cell lysates using an anti-GFP antibody. Equivalent amounts of total protein extracts (T), depleted supernatants (S), and a 10-fold equivalent of the immune pellets (P) were analyzed by Western blotting using anti-GFP (a) or anti-HA (a′, b′, and c′) antibody. The results with the GFP antibody were similar in all experiments and are presented only for the strain expressing HA-Nup133a. Molecular mass markers are on the right in kilodaltons. (B) Silver staining of immunoprecipitates from control, GFP-SpNup85, GFP-Seh1, and Nup107-GFP cell extracts obtained with an anti-GFP antibody. The asterisks indicate the position of the GFP fusion in each lane. The dots indicate additional bands subsequently identified by mass spectrometry as Nup145-C (band 1) and Nup85 (band 2). (C) Schematic model of the Nup107-120 complex in *S. pombe*, based on the structural data obtained from *S. cerevisiae* (38).

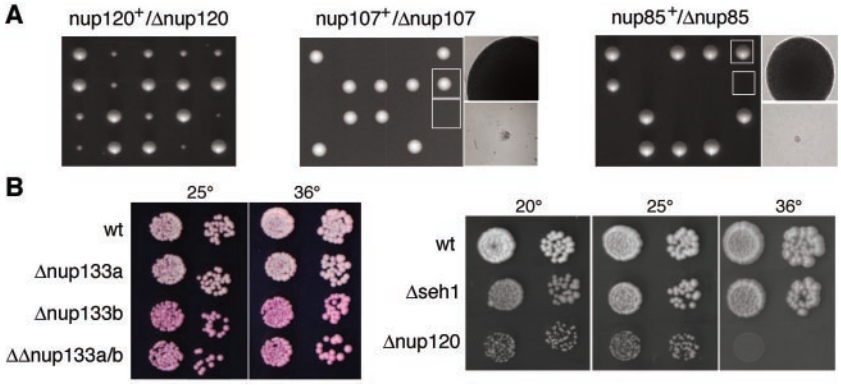

FIG. 3. Growth properties of mutant strains with disrupted Nup107-120 complex nucleoporin genes. (A) Tetrads from *nup120*$^+$/Δ*nup120*, *nup107*$^+$/Δ*nup107*, and *nup85*$^+$/Δ*nup85* heterozygous diploids were dissected and incubated on YE5S plates at 25°C for 5 days. Higher-magnification images of *nup107*$^+$, Δ*nup107*, *nup85*$^+$, and Δ*nup85* colonies (boxed) are also shown (insets). (B) Serial dilutions of *S. pombe* cells carrying *nup133a*, *nup133b*, *seh1*, and *nup120* deletions or a combined deletion of both *nup133a* and *nup133b* (ΔΔ*nup133a*/*b*) were spotted onto YE5S plates containing phloxine-B at the indicated temperatures. wt, wild type.

ScNup133 appears to be loosely associated with the ScNup84 complex (2, 38). Despite this difference, we will subsequently designate this subset of nucleoporins as constituents of the *S. pombe* Nup107-120 complex by analogy to the vertebrate Nup107-160 complex.

The *S. pombe* null mutant strains display different viability phenotypes than their *S. cerevisiae* counterparts. To investigate the functions of constituents of the SpNup107-120 complex, null alleles were generated (see Materials and Methods). As in *S. cerevisiae*, deletion of *S. pombe nup120* leads to a temperature-sensitive phenotype (Fig. 3B, right). In contrast, spores carrying the Δ*nup107* or Δ*nup85* allele, while able to germinate at 25°C, formed microcolonies of only ~20 to 60 cells (equivalent to four to six divisions) (Fig. 3A). This indicated that, unlike their *S. cerevisiae* counterparts, *nup107* and *nup85* are required for vegetative growth in *S. pombe*. Conversely, while deletion of *S. cerevisiae SEH1* leads to a cold-sensitive phenotype (59), analysis of *S. pombe* Δ*seh1* cells did not reveal any detectable growth defect in a range of temperatures from 16 to 36°C (Fig. 3B and data not shown). Single or combined deletion of the *nup133a* and *nup133b* genes did not lead to any major growth defect at any temperature tested (16 to 36°C). However, phloxine B-containing plates revealed an increased intracellular accumulation of this vital dye in cells disrupted for *nup133b* but not *nup133a*, indicating that deletion of *nup133b* slightly impairs cell viability at all temperatures (Fig. 3B).

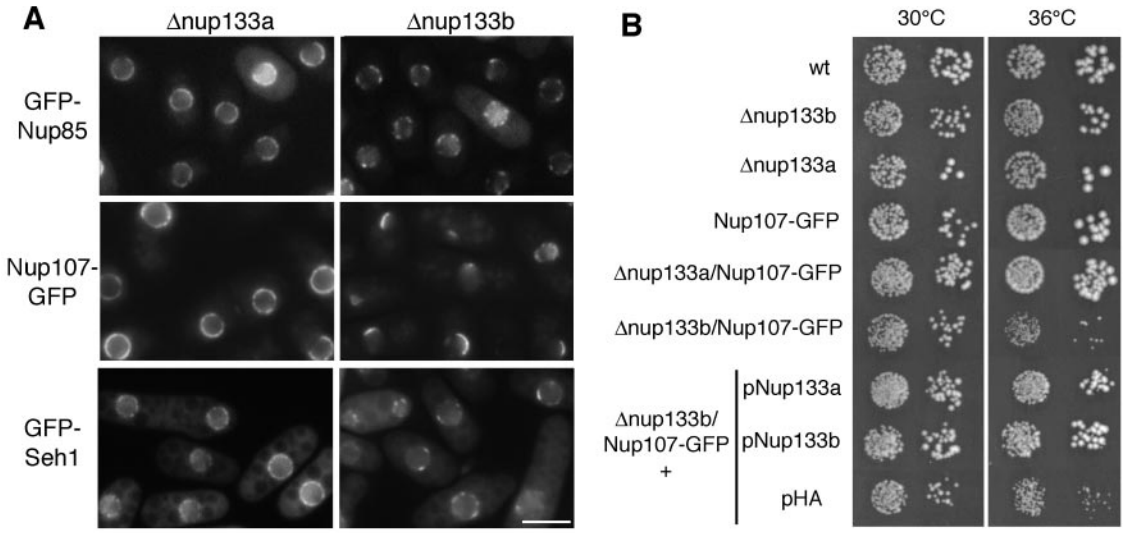

FIG. 4. Localization of GFP-tagged nucleoporins in Δ*nup133a*, Δ*nup133b*, and Δ*nup120* mutants reveals NPC aggregation and specific genetic interactions within the Nup107-120 complex. (A) In vivo localization of GFP-Nup85, Nup107-GFP, and GFP-Seh1 in Δ*nup133a* and Δ*nup133b* strains. The cells were grown at 30°C on YE5S plates. Bar, 5 μm. In contrast to Δ*nup133a* cells, Δ*nup133b* cells display a heterogeneous distribution of the GFP fusions, which is particularly pronounced in the case of Nup107-GFP. (B) Serial dilutions of wild-type (wt), Δ*nup133b*, *nup107*-GFP, Δ*nup133b*/*nup107*-GFP, and Δ*nup133a*/*nup107*-GFP cells were spotted onto YE5S medium and grown for 4 days at 30°C or for 3 days at 36°C. The growth of Δ*nup133b*/*nup107*-GFP cells carrying (+) a pREP3-HA-Nup133b, pREP3-HA-Nup133a, or pREP3-HA plasmid further indicates that the temperature-dependent growth defect of the Δ*nup133b*/*nup107*-GFP mutant can be rescued by Nup133b, as well as Nup133a.

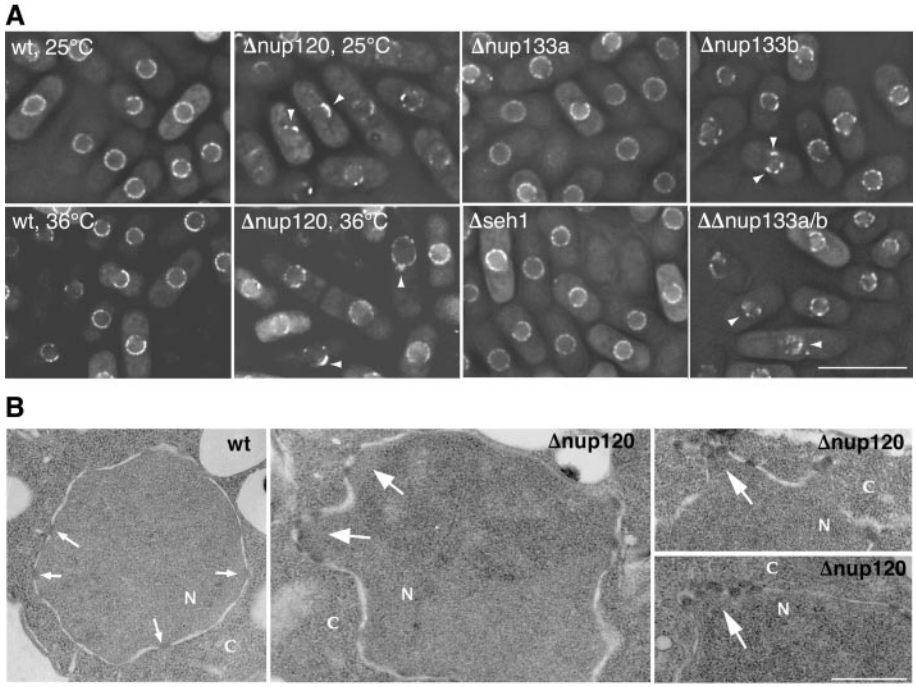

FIG. 5. Alterations of NPC distribution in Δ*nup133b* and Δ*nup120* cells. (A) In vivo distribution of GFP-Nsp1^{Sp} expressed from the *nmt1*** (low-strength) promoter. Wild-type (wt), Δ*seh1*, Δ*nup133a*, *nup133b*, Δ*nup133a*/Δ*nup133b*, and Δ*nup120* cells expressing GFP-Nsp1^{Sp} were grown on thiamine-free EMM plates at 25°C or, when indicated, incubated for 6 h at 36°C, and the localization of the fusion protein was examined in live cells. Representative deconvolved images are shown. The arrowheads point to NPC clusters. Bar, 10 μm. (B) Thin-section electron micrographs of wild-type and Δ*nup120* cells grown at semipermissive temperature (30°C). The small arrows point to NPCs. Nuclear pore clusters in the Δ*nup120* mutant are indicated by large arrows. N, nucleus; C, cytoplasm. Bar, 200 nm.

Nup133b and Nup120 are required for normal NPC distribution in *S. pombe*. Since deletions of members of the *S. cerevisiae* Nup84 complex cause severe defects in the distribution and organization of NPCs, we analyzed NPC distribution in *S. pombe* strains carrying deletions of the nonessential constituents of the Nup107 complex by combining deletion of the *nup133a* or *nup133b* gene with an integrated copy of GFP-Nup85, GFP-Seh1, or Nup107-GFP. As shown in Fig. 4A, a homogeneous punctate perinuclear distribution of these nucleoporins, similar to that observed in wild-type cells (Fig. 1), was observed in a Δ*nup133a* strain. In contrast, a clear clustering phenotype was observed with Nup107-GFP, GFP-Nup85, or GFP-Seh1 in Δ*nup133b* cells, which was more pronounced in the Δ*nup133b* strain expressing Nup107-GFP. This Δ*nup133b*/*nup107*-GFP strain also displays growth defects at 36°C, a temperature at which the individual *nup107*-GFP and Δ*nup133b* strains grow very well (Fig. 4B). In contrast, the Δ*nup133a*/*nup107*-GFP, Δ*nup133b*/GFP-*nup85*, and Δ*nup133b*/GFP-*seh1* strains are not temperature sensitive (Fig. 4B and data not shown). It thus appears that GFP tagging of Nup107 at its C terminus, although capable of complementing the lethal phenotype of Δ*nup107* and allowing biochemical interactions with at least Nup133a and Nup133b, may slightly impair its function. The temperature-sensitive phenotype of the Δ*nup133b*/*nup107*-GFP strain could be complemented by HA- or GFP-tagged Nup133b (Fig. 4B and data not shown), but surprisingly, also by HA- or GFP-tagged Nup133a expressed under the control of the *nmt1* promoter in the presence of thiamine, which does not completely eliminate expression (i.e., conditions similar to those used for Fig. 2). This suggests that endogenous Nup133a is expressed at very low levels in wild-type cells and indicates that its mild overexpression can overcome some of the defects caused by the *nup133b* deletion (see Discussion).

Attempts to obtain Δ*nup120* strains carrying an integrated copy of Nup107-GFP or GFP-Nup85 revealed mild and severe synthetic lethality, respectively. As an alternative approach to follow NPC distribution, mutant strains were transformed with a plasmid encoding a fusion between GFP and the *S. pombe* homologue of ScNsp1p (Nsp1^{Sp}) (74). As shown in Fig. 5A, a homogeneous ring-like staining of the nuclear periphery was observed in wild-type, Δ*seh1*, and Δ*nup133a* strains. In contrast, Δ*nup133b* and Δ*nup133a*/Δ*nup133b* cells gave a discontinuous, patchy ring around the NE, and an even stronger phenotype was observed in Δ*nup120* cells, in which fewer bright spots were observed at the nuclear periphery in most cells grown at 25°C, and to a lesser extent at 36°C (Fig. 5A). In these strains, a more pronounced phenotype was observed when cells were grown on plates, suggesting that, as previously reported for several *S. cerevisiae* mutants (8, 27, 45), the extent of NPC clustering depends on growth conditions. Finally, thin-section electron microscopy confirmed the nonhomogeneous NPC distribution in Δ*nup120* cells and revealed, in some cases, minor alterations of NE structure (Fig. 5B).

Mutations in the SpNup107-120 complex affect the export of poly(A)$^+$ RNAs. To analyze the subcellular distribution of poly(A)$^+$ RNAs in the various mutant strains, FISH exper-

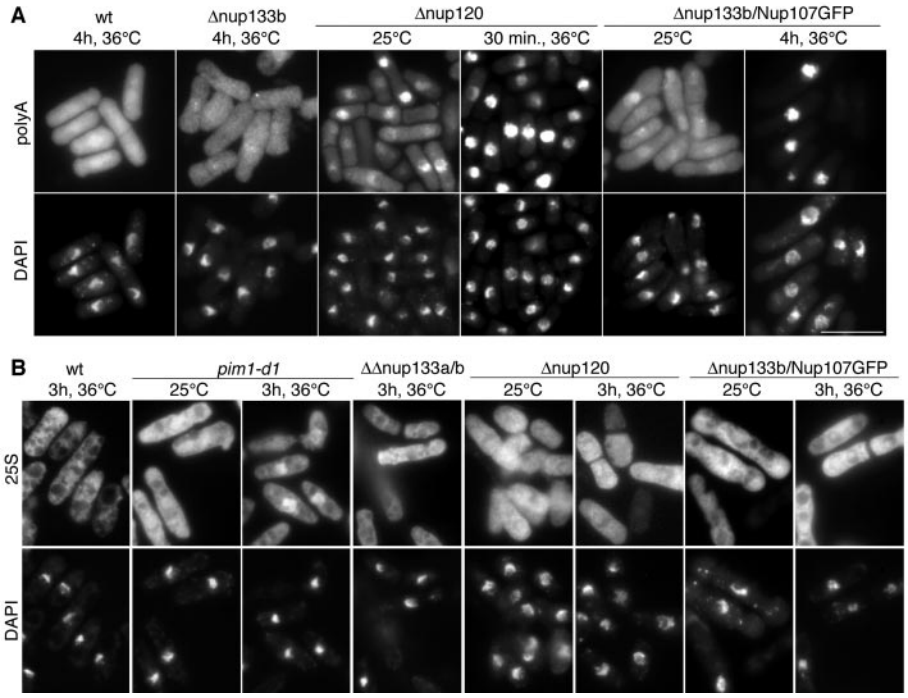

FIG. 6. Mutations in the Nup107-120 complex cause mRNA export defect. (A) Rapid accumulation of poly(A)$^+$ RNA in Δ*nup120* and Δ*nup133b*/*nup107*-GFP mutants at restrictive temperature. Wild-type (wt), Δ*nup133b*, Δ*nup120*, and Δ*nup133b*/*nup107*-GFP strains grown at 25°C or shifted to 36°C were fixed and subjected to in situ hybridization with a Cy3-labeled oligo(dT)$_{50}$ probe. DNA was stained with DAPI. Bar, 10 μm. (B) Distribution of the pre-60S ribosomal particles in Nup107-120 complex mutants. Strains grown at 25°C or shifted to 36°C for 3 h were processed for FISH using a Cy3-labeled probe complementary to the 25S rRNA.

iments were performed. In wild-type and Δ*nup133b* cells, poly(A)$^+$ RNAs were uniformly distributed throughout the cells at both 25 and 36°C (Fig. 6A). In contrast, Δ*nup120* cells grown at 25°C already accumulate poly(A)$^+$ RNA inside their nuclei. In these cells, a clear nuclear poly(A)$^+$ RNA signal was observed in ~30% of the cells within 10 min at 36°C (data not shown) and in most cells by 30 min (Fig. 6A). A similar, albeit less severe, phenotype was also observed in Δ*nup133b*/*nup107*-GFP cells, in which nuclear accumulation of poly(A)$^+$ RNA could be observed in ~40% of the cells following a 1-h shift to 36°C (data not shown) and in most of these cells after 4 h at 36°C (Fig. 6A). Therefore, both Δ*nup120* and Δ*nup133b*/*nup107*-GFP strains exhibit a poly(A)$^+$ RNA export defect.

We also analyzed the nuclear export of the pre-60S ribosomal particles using probes complementary to the 25S rRNA. As a control, we used the *pim1-d1* strain that carries a mutation in the nucleotide exchange factor for the small GTPase Ran^{Sp}/Spi1 (56). In agreement with data obtained from *S. cerevisiae* (34), nuclear retention of 25S rRNA was observed in the temperature-sensitive *pim1-d1* strain (Fig. 6B). In contrast, no detectable intranuclear accumulation of pre-60S particles could be detected in the Δ*nup120*, Δ*nup133b*/*nup107*-GFP, or ΔΔ*nup133a*/*b* strain (Fig. 6B). Although one cannot formally exclude a minor defect in pre-60S rRNA export, this result suggests that the poly(A)$^+$ RNA export defect observed in the *S. pombe* Nup107-120 mutant strains is specific and does not reflect a general impairment of nucleocytoplasmic transport in these strains.

Δ*nup120* and Δ*nup133b*/*nup107*-GFP mutant strains exhibit severe cell division defects at restrictive temperature. Unexpectedly, microscopic analyses of Δ*nup120* cells, and to a lesser extent Δ*nup133b*/*nup107*-GFP cells, revealed cell division defects at the restrictive temperature. In these cells, calcofluor staining of asynchronous cultures showed an increase of the septation index upon incubation at 36°C. In Δ*nup120* cells, ~40% had a septum after a 3- or 6-h shift to 36°C compared to ~10% of wild-type cells or Δ*nup120* cells grown at 25°C (Fig. 7A). Moreover, Δ*nup120* cells exhibited septation defects (i.e., widened, misplaced, or occasionally, multiple septa) even at 25°C (~10% of the septa) and more frequently at 36°C (~20% of the septa at 3 h and ~40% at 6 h) (Fig. 7A). To further characterize this cytokinesis defect, wild-type or Δ*nup120* cells synchronized in G_1/S at 25°C using hydroxyurea were released at 36°C upon hydroxyurea washout. Under these conditions, we observed an ~1-h delay of septation onset in Δ*nup120* cells compared to wild-type cells and the aberrant persistence of septated cells (data not shown).

DAPI staining also revealed aberrant mitoses, such as unequally segregated chromosomes and lagging chromosomes, in Δ*nup120* cells shifted for 3 or 6 h to 36°C (Fig. 7A and 8; see below). We also detected many mononucleated Δ*nup120* cells showing hypercondensed chromatin, suggesting a lag at metaphase in the Δ*nup120* mutant. In binucleated and septated Δ*nup120* cells that accumulate at 36°C, atypical DAPI staining patterns were frequently observed (Fig. 7A). Flow cytometry analyses showed that while Δ*nup120* cells mainly have a 2C DNA content at 25°C, 4C-containing cells accumulated at 36°C (Fig. 7B), indicating that DNA replication had occurred. Finally, the NLS–GFP–β-galactosidase reporter accumulated efficiently in the nuclei of Δ*nup120* cells at both permissive and

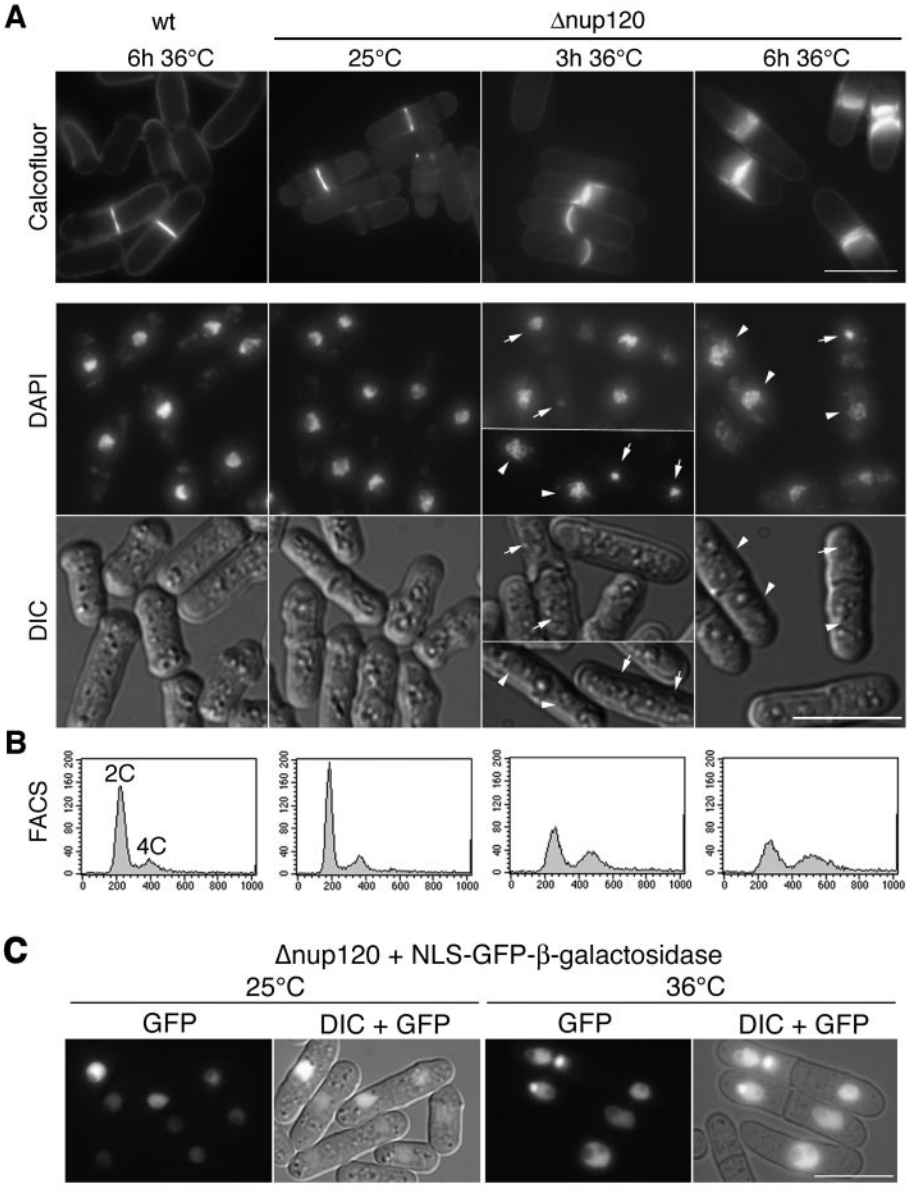

FIG. 7. Δ*nup120* strain accumulates binucleated cells with abnormal septa and hypercondensed chromatin at 36°C. (A) Samples from wild-type (wt) and Δ*nup120* cells grown at 25°C or shifted for 3 or 6 h to 36°C were fixed and stained with calcofluor or DAPI as indicated. The differential interference contrast (DIC) image of the DAPI-stained cells revealing the presence of the septum is also shown. The arrows indicate septated Δ*nup120* cells with condensed or unequally segregated chromosomes. The arrowheads point to nuclei with atypical DAPI staining patterns. Bar, 10 μm. (B) Samples from the same cultures were stained with propidium iodide and analyzed by FACS. The fluorescence (the DNA content on an arbitrary scale) and frequency (relative cell number) are plotted along the *x* and *y* axes, respectively. Relative fluorescences corresponding to 2C and 4C DNA contents are indicated. (C) The localization of the NLS–GFP–β-galactosidase fusion was monitored in living Δ*nup120* cells grown at 25°C or incubated for 3 h at 36°C. Bars, 10 μm.

restrictive temperatures (Fig. 7C), indicating that unlike several mutant alleles defective in the Ran^{Sp}/Spi1pathway (53), NE integrity is not impaired in Δ*nup120* cells.

Altogether, our results indicate that Δ*nup120* cells shifted to 36°C are at least transiently blocked at metaphase, leading to a delay in septation onset. After the first nuclear division, these cells can proceed to septum formation, replicate their DNA, and accumulate as septated cells with an intact NE but an atypical chromatin structure.

To further characterize these mitotic defects, Δ*nup120* and wild-type cells grown at 25°C or shifted to 36°C for 3 or 6 h were analyzed by immunofluorescence using an anti-tubulin antibody and DAPI. Analysis of the various stages of mitosis, assessed by the length of the mitotic spindle, revealed an increased proportion of Δ*nup120* cells in premetaphase and metaphase after 3 h at 36°C compared to wild-type cells or Δ*nup120* cells grown at permissive temperature (Fig. 8A and C). In addition, this study revealed that even in cells grown at 25°C, ~20% of the mitotic Δ*nup120* cells had undergone aberrant mitoses. At 36°C, this proportion reached ~70% of the

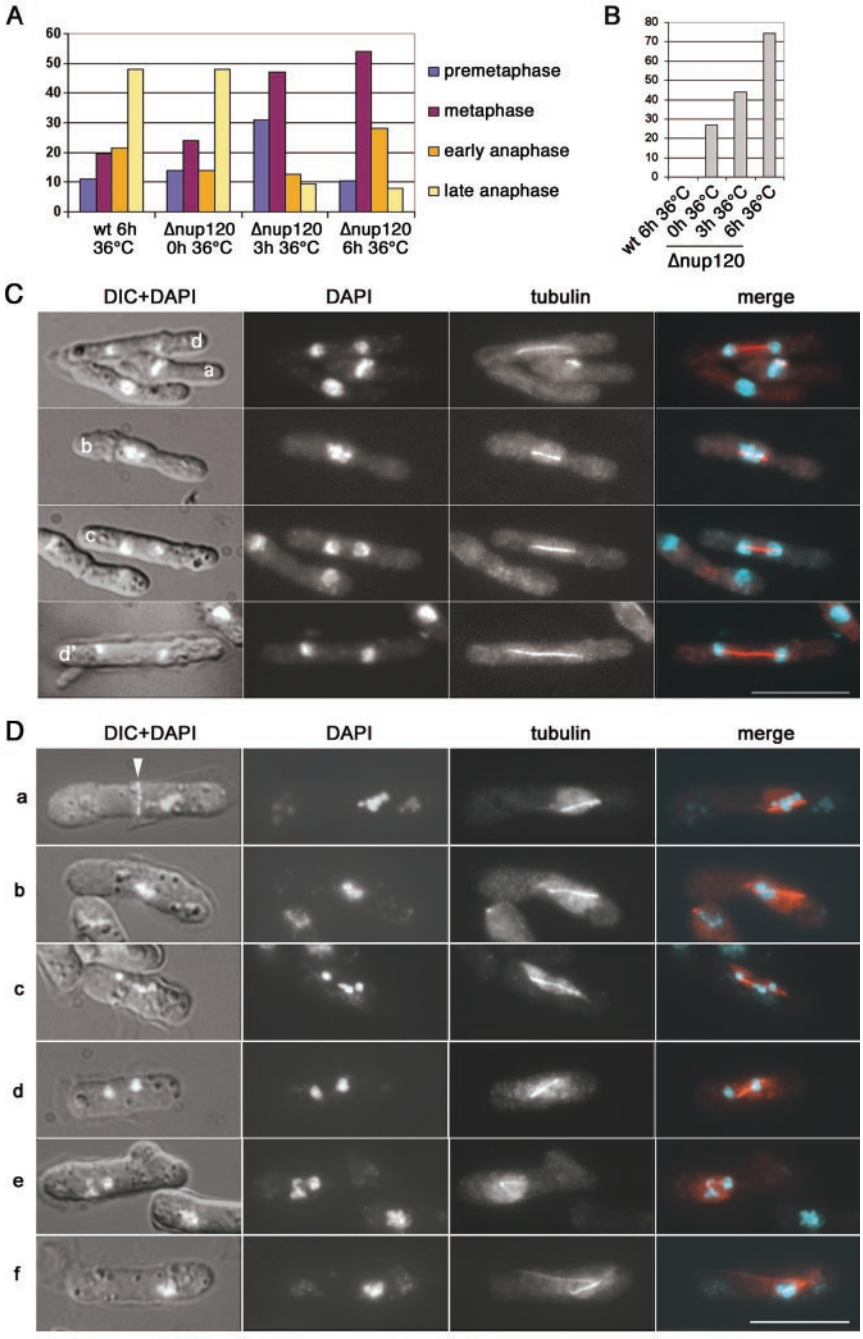

FIG. 8. Δ*nup120* cells display abnormal microtubule spindles and aberrant mitosis. Wild-type (wt) and Δ*nup120* cells grown asynchronously at 25°C or shifted to 36°C for 3 or 6 h were processed for immunofluorescence using the TAT1 antibody to visualize microtubules and DAPI to observe the DNA morphology. (A) The frequencies of the different stages of mitosis were determined according to the lengths of the mitotic spindles (panel C). An average of 40 mitoses were examined for each sample, and a χ^2 procedure was applied for statistical analysis (wt/Δ*nup120* at 0 h and 36°C, P = not significant; wt/Δ*nup120* at 3 h and 36°C, $P \leq 0.001$; wt/Δ*nup120* at 6 h and 36°C, $P \leq 0.001$). Note that the increase in the early anaphase stage observed in Δ*nup120* cells after a 6-h shift to 36°C may reflect the accumulation of abnormal metaphases with aberrant spindle lengths. (B) The percentage of abnormal mitoses was also quantified. (C) Prometaphase (a), metaphase (b), and early (c) and late (d and d′) anaphase in Δ*nup120* cells grown at 25°C. (D) Examples of abnormal mitoses exhibited by Δ*nup120* cells shifted for 6 h to 36°C. Rows: a, misplaced nucleus or spindle; b, chromosome missegregation; c, lagging chromosomes; d, chromosomes unattached to the spindle; e, monopolar spindle; f, malformed mitotic spindle. For each example, images of DIC combined with DAPI (DIC+DAPI), DAPI, tubulin staining, and DAPI plus tubulin staining (merge) are shown. In row a, the medial plane of septation was visualized using anti-Mid1 immunostaining (arrowhead). Bar, 10 μm.

mitotic cells after a 6-h shift to 36°C (Fig. 8B and D) ($P \leq 0.01$). Aberrant mitoses included displaced positioning of the nucleus and microtubule spindle relative to the long axis of the cell, with the three condensed chromosomes displaced from the center of the cell (Fig. 8D, a and f); unequal sister chromatid segregation; lagging or unattached chromosomes (Fig. 8D, b, c, and d); and compromised microtubule structures (monopolar spindles and misshaped spindles) (Fig. 8D, e and f).

Accurate chromosome transmission is defective in a Δ*nup120* strain. As many mutants with altered spindle assembly and function show hypersensitivity to microtubule-depolymerizing agents, such as TBZ, we performed serial cell dilutions on rich medium containing various concentrations of TBZ. As shown in Fig. 9A, 10 μg of TBZ/ml severely inhibited the growth of the Δ*nup120* mutant at permissive temperature (23°C) compared to wild-type cells, indicating that *nup120* deletion affects, most likely indirectly, microtubule integrity or spindle function. We then determined if the spindle checkpoint, which monitors mitotic spindle integrity and attachment of the kinetochores to the spindle, was required for the viability of the Δ*nup120* strain. Strains with both *nup120* and either of the spindle checkpoint genes, *mph1* (29) or *mad2* (30), deleted were viable. Unlike single mutants, Δ*nup120*/Δ*mph1* cells were sensitive to 5 μg of TBZ/ml at 23°C, indicating a synergistic effect of the two mutations (Fig. 9A). In contrast, sensitivity to TBZ was indistinguishable in Δ*nup120* and Δ*nup120*/Δ*mad2* mutants. This pattern of synthetic interaction with Δ*mph1* but not with Δ*mad2* is similar to that seen with a point mutant of *spi1* (18) and likely reflects differences in the severities of the spindle checkpoint defects in the two mutant strains.

To analyze chromosome segregation in Δ*nup120* cells in more detail, we monitored the presence of a nonessential minichromosome (47) whose loss results in adenine auxotrophy and the subsequent appearance of pink colonies on plates containing low adenine. However, attempts to isolate an *S. pombe* Δ*nup120* strain containing this minichromosome were not successful. Furthermore, while the Δ*nup120* strain transformed by a complementing pUra4-Nup120 plasmid was able to lose the plasmid and thus to grow on 5-FOA-containing plates at the permissive temperature, Δ*nup120* cells carrying pUra4-Nup120 and a minichromosome failed to grow on 5-FOA (Fig. 9B). Accordingly, the presence of an additional chromosome in a Δ*nup120* mutant severely impairs cell viability. Similar results were previously reported in the case of the *alp14* mutant and were interpreted as resulting from extreme instability of the minichromosome (25).

As an alternative approach, we followed chromosome segregation in a heterozygous Δ*nup120*/*nup120*$^+$ h^+/h^+ *ade6-M210*/*ade6-M216* (Ade$^+$) diploid by monitoring the loss of one *ade6* mutant allele that leads to the appearance of pink colonies. This diploid strain is homozygous at the mating-type locus and consequently is incompetent for meiosis. Interestingly, a significant increase in the number of pink (Ade$^-$) colonies was observed in a Δ*nup120*/*nup120*$^+$ diploid grown at 36°C compared to a wild-type *nup120*$^+$/*nup120*$^+$ strain or a Δ*nup120*/*nup120*$^+$ diploid grown at 30°C (Fig. 9C). Flow cytometric analysis of the DNA content revealed that the pink-colony cells had mainly a 2C DNA content, in contrast to the white-colony cells, which were 4C (data not shown). Such a "haploidization" phenotype (loss of the disomic state for all three chromosomes as a consequence of initial loss of one chromosome in *S. pombe* diploids) was previously described (46) and is very similar to that previously reported in the case of a Δ*spi1*/*spi1*$^+$ diploid (40, 53). Our data thus demonstrate that Nup120 is essential for genome stability and integrity during mitosis.

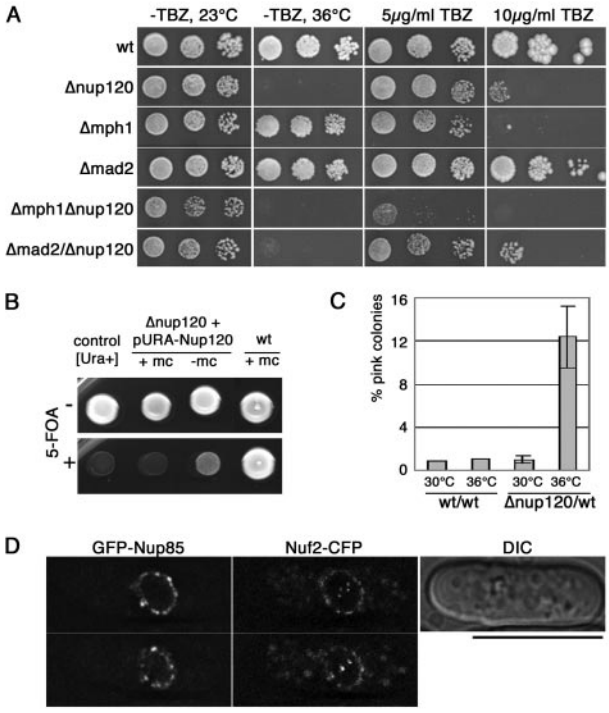

FIG. 9. Hypersensitivity to TBZ and chromosome segregation defects in Δ*nup120* cells. (A) Deletion of *nup120* induces hypersensitivity to the microtubule-destabilizing drug TBZ. Serial dilutions of wild-type (wt) and mutant cells were spotted on YE5S medium containing or lacking (−) TBZ (5 or 10 μg/ml) and incubated at 23°C. A TBZ-free plate was also incubated at 36°C. Note that the TBZ sensitivity of the Δ*nup120* cells is further enhanced in a Δ*mph1* background. (B) The presence of a minichromosome is toxic in Δ*nup120* haploid cells. Δ*nup120* strains complemented by the pUra-Nup120 plasmid and containing (+mc) or lacking (−mc) a minichromosome were spotted on supplemented EMM plates in the presence or absence of 5-FOA at 23°C. Δ*nup120* cells that carry both pUra-Nup120 and a minichromosome cannot grow on 5-FOA, indicating that the pUra-Nup120 plasmid cannot be easily lost by these cells. (C) Δ*nup120*/wt heterozygous diploid cells undergo chromosome loss at 36°C. wt/wt h^+/h^+ *ade6-M210*/*ade6-M216* (wt/wt) and Δ*nup120*/*wt* h^+/h^+ *ade6-M210*/*ade6-M216* (Δnup120/wt) diploids were plated on low-adenine yeast extract medium at 30 or 36°C. The percentage of pink [Ade$^-$] colonies that had lost one of the two *ade6* alleles was determined. The average of four independent experiments is presented. The error bars represent standard deviations. (D) Unlike Nuf2-CFP, GFP-Nup85 is not detectable at kinetochores in metaphase-arrested cells. *nuc2-663* cells with integrated copies of both GFP-Nup85 and Nuf2-CFP were arrested in metaphase by a 3-h shift to 36°C. Deconvolved images of two Z sections (0.6 μm apart) of a live cell are presented. The perinuclear labeling observed in the CFP channel is due to the bleedthrough of the GFP-Nup85 signal. The DIC image of the cell is also shown. Bar, 10 μm.

Because several constituents of the human Nup107 complex are localized at kinetochores during mitosis (7, 28), it was tempting to link these defects in chromosome segregation to a possible function of this complex at kinetochores. To determine whether the *S. pombe* Nup107 complex is similarly localized at kinetochores during mitosis, we analyzed the

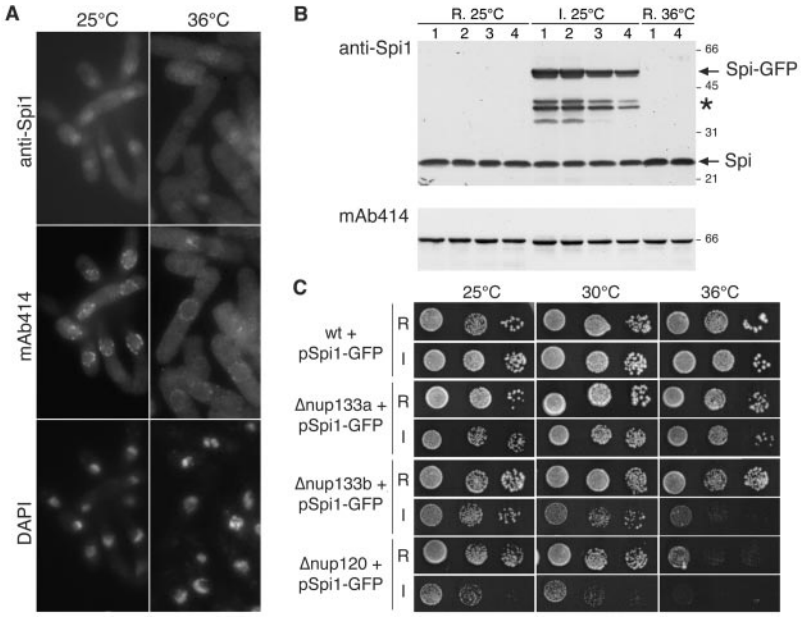

FIG. 10. Localization of endogenous Spi1 and toxicity of Spi1-GFP in Nup107-120 complex nucleoporin mutants. (A) Δ*nup120* cells grown at 25°C or shifted for 4 h to 36°C were processed for immunofluorescence using affinity-purified anti-Spi1 antibody, mAb414 antibody to visualize the NPCs, and DAPI to visualize the DNA. Note that in the Δ*nup120* strain at both 25 and 36°C, the nuclear pores surround the DNA and Spi1 is predominantly but not exclusively localized to the nucleus. Despite the overall weaker Spi1 and mAb414 signals at 36°C, moderate changes in the intracellular distribution of Spi1 can be observed in Δ*nup120* cells shifted to the restrictive temperature. (B) Wild-type (lanes 1), Δ*nup133a* (lanes 2), Δ*nup133b* (lanes 3), and Δ*nup120* (lanes 4) cells expressing the Spi1-GFP fusion under the control of the *nmt1** promoter were grown at 25°C in liquid EMM supplemented with thiamine (repressed [R] *nmt1* promoter, R. 25°C) and shifted either for 24 h at 25°C to thiamine-free medium (induced [I] *nmt1* promoter, I. 25°C) or for 4 h to 36°C in thiamine-containing medium (R. 36°C). Equivalent amounts of whole-cell lysates were analyzed by Western blotting using anti-Spi1 antibody. The same blot was reprobed with the mAb414 antibody that mainly recognized a protein most likely corresponding to $Nsp1^{Sp}$ (theoretical mass, 61 kDa; GeneDB database). Note that the levels of endogenous Spi1 are similar in wild-type (lanes 1) and Δ*nup120* (lanes 4) cells even when shifted to 36°C (R. 36°C), whereas the expression levels of Spi1-GFP and its degradation products (*) are lower in Δ*nup133b* (lanes 3) and Δ*nup120* (lanes 4) strains grown at 25°C in thiamine-free liquid medium (I. 25°C). (C) Spi1-GFP expression is toxic in Δ*nup120* and Δ*nup133b* mutant cells. Wild-type (wt), Δ*nup133a*, Δ*nup133b*, and Δ*nup120* cells expressing the Spi1-GFP fusion under the control of the *nmt1** promoter were grown to mid-log phase in liquid EMM supplemented with thiamine. The cells were then either spotted onto EMM-plus-thiamine plates (repressed *nmt1* promoter) or shifted for 24 h at 25°C to thiamine-free liquid medium and spotted on thiamine-free EMM (induced *nmt1* promoter). The plates were incubated at 25, 30, or 36°C.

localization of GFP-Nup85 in metaphase-arrested cells, taking advantage of the *nuc2-663* mutation (32). In addition, we used the Nuf2-CFP marker (24) to visualize kinetochore positioning. In the resulting GFP-*nup85*/*nuf2*-CFP/*nuc2-663* cells, intranuclear Nuf2-CFP dots were clearly detected in metaphase. However, while GFP-Nup85 gave a bright localization at the nuclear rim, no specific labeling could be observed at kinetochores (Fig. 9B). Although the presence of undetectable amounts of GFP-Nup85 at kinetochores cannot be excluded, this result suggests that kinetochore localization of the Nup107 complex might be restricted to higher eukaryotes.

The SpNup107-120 complex is functionally and genetically linked to the Ran^{Sp}/Spi1 pathway. While this study was in progress, Gao and coworkers reported that nuclear accumulation of the small GTPase Ran^{Sc}/Gsp1p was impaired in *S. cerevisiae* Δ*nup133*, *nup120-1*/*rat2-1*, and Δ*nup85* mutant strains (23). These results, together with the similarity of cell cycle defects observed in the *S. pombe* Δ*nup120* strain and several mutants defective in the Ran^{Sp}/Spi1 pathway, prompted us to analyze whether alteration of the Spi1 pathway could be responsible for some of the defects observed in Δ*nup120* mutant cells. We therefore investigated the expression level and distribution of Spi1 in Δ*nup120* strains grown at permissive temperature or shifted for 4 h to 36°C. Western blot analysis did not reveal any significant alteration of the expression level of endogenous Spi1 in Δ*nup120* cells grown at 36°C (Fig. 10B, compare R. 25°C and R. 36°C, lanes 1 and 4). Upon fluorescence analysis, both the Spi1 and mAb414 signals were reproducibly fainter in the Δ*nup120* strain at 36°C (Fig. 10A). However, since (i) NE targeting of GFP-$Nsp1^{Sp}$ is not significantly altered in Δ*nup120* cells at 36°C (Fig. 5A) and (ii) the expression level of neither endogenous Spi1 nor the major 65-kDa protein (most likely $Nsp1^{Sp}$) recognized by the mAb414 antibody is affected (Fig. 10B), this decreased staining most likely reflects technical limitations associated with the efficiency of fixing or spheroplasting these cells once they are grown at 36°C. Despite the weaker overall staining, fluorescence analysis revealed moderate changes in the distribution of Spi1 in Δ*nup120* cells shifted to the restrictive temperature: although a nuclear signal remained detectable in most cells, the relative signal for Spi1 in the nucleus relative to the cytoplasm was lower in cells grown at the restrictive temperature (Fig. 10A).

It has been reported that mutations in several genes of the Ran^{Sp}/Spi1 pathway, such as *pim1* and *mog1*, are rescued by overexpression of wild-type Spi1 (40, 56, 63). Using the

pREP3X-Spi1 plasmid (42), we could not observe any rescue of either cell growth or septation defects of Δ*nup120* cells at 36°C (data not shown). However, this study revealed that expression of Spi1-GFP under the control of the medium-strength *nmt1* (*nmt1**) promoter (Fig. 10B) enhanced the growth defect of Δ*nup120* cells and decreased the viability of Δ*nup133b* mutant cells (Fig. 10C). In contrast, the growth properties of wild-type and Δ*nup133a* cells were not altered by Spi1-GFP expression. As the Spi1-GFP fusion is not functional (63), its expression, although not affecting wild-type cell growth, may lead to a competition with endogenous Spi1 in Δ*nup120* and Δ*nup133b* mutants. Most likely correlated with this toxicity, we reproducibly found that the expression level of Spi1-GFP was lower in both Δ*nup133b* and Δ*nup120* cells (Fig. 10B). These data thus strengthen the functional link between the Nup107-120 complex and the Spi1/Ran pathway.

DISCUSSION

The evolutionarily conserved ScNup84/vertebrate Nup107-160/SpNup107-120 complex: conservation and divergences. In this study, we have identified and functionally characterized *S. pombe* nucleoporins homologous to components of the ScNup84/vertebrate Nup107-160 complex. Unexpectedly, the *S. pombe* genome contains two ORFs encoding Nup133 orthologues, which we designated Nup133a and Nup133b. Sequence analysis indicated that the corresponding proteins were nearly as divergent from each other (19.5% homology between SpNup133a and SpNup133b) as they are from their *S. cerevisiae* or human counterparts (Table 2), yet the two nucleoporins were both targeted to the NPCs and able to interact with Nup107. Although single or combined deletion of *nup133a* and *nup133b* did not affect cell viability, Nup133b appeared to have a function that was predominant over Nup133a: unlike deletion of *nup133a*, deletion of *nup133b* led to (i) minor growth defects; (ii) synergistic growth defects when combined with *nup107*-GFP, Δ*nup120*, or Δ*nup184* (whose product is the *S. pombe* homologue of ScNup188p [71]) (Fig. 4 and data not shown); and (iii) toxicity of Spi1-GFP expression. Despite the lack of any detectable function of the *nup133a* gene, its overexpression was able to complement the phenotypes induced by *nup133b* deletion. Although Nup133a may have a specific function that was not revealed by our assays, a more likely explanation is that, under some conditions, the protein may provide a backup pool for Nup133 function. In this respect, it is noteworthy that Nup133a appears to be mildly induced (2- to 2.5-fold) under several stress conditions (H_2O_2, cadmium, or heat), a feature that is not shared by any other constituent of the Nup107-120 complex (11; http://www.sanger.ac.uk/PostGenomics/S_pombe/projects/stress/).

Another unexpected result arising from this study was the lack of a major growth defect induced by *Spnup133a/b* deletions that differs from the temperature-sensitive phenotype induced by *NUP133* deletion in *S. cerevisiae* (17, 37, 50) and the essential function of Nup133 in vertebrate NPC assembly (68). Yet, Nup133 inactivation in *Caenorhabditis elegans* does not lead to any major defect (reference 22 and references therein). More generally, comparison of the phenotypes obtained upon deletion of *S. cerevisiae* and *S. pombe* genes, or induced by RNA interference in *C. elegans* (reference 22 and references therein) or in human cells (9, 28, 68), revealed major divergences among these organisms. The fact that the viability phenotypes were as divergent between the two yeasts as with either *C. elegans* or vertebrates suggests that these differences reflect the evolution of individual nucleoporins within the ScNup84, SpNup107-120, and metazoan Nup107-160 complexes rather than specific features of evolutionarily divergent organisms (i.e., both of the yeasts that undergo a closed mitosis versus metazoans with an open mitosis).

In summary, although in certain instances some of its individual constituents might be dispensable for cell viability or less tightly associated with other subunits, the evolutionarily conserved ScNup84/SpNup107-120/metazoan Nup107-160 complex appears to be required, as an entity, for cell viability in all organisms tested to date.

The major functions of the ScNup84/SpNup107-120 complexes have been evolutionary conserved. Despite the divergence observed at the level of individual nucleoporins, functional analysis of several of the *S. pombe* mutant strains revealed a disturbed NPC distribution, similar to the phenotypes previously reported for *S. cerevisiae* constituents of the Nup84 complex. Although the NPC clustering phenotype is not as pronounced in *S. pombe* as in several *S. cerevisiae* mutants, these newly identified *S. pombe* mutants provide a useful tool to discriminate NE- from NPC-associated proteins. In addition, FISH studies revealed nuclear accumulation of poly(A)$^+$ RNA at the restrictive temperature in the Δ*nup120* and Δ*nup133b*/*nup107*-GFP mutants. Our study also revealed major mitotic defects associated with mutations within the Nup107-120 complex. Although not extensively characterized, mitotic defects were also previously reported in *S. cerevisiae* Δ*nup120* (1) and Δ*nup84* strains (59). It is noteworthy that the dual function of the SpNup107-120/ScNup84 complex in mRNA export and the cell cycle represents an additional example of potential linkage between these two pathways: while Rae1, initially identified as an mRNA export factor, was also shown to be required for proper mitosis in both *S. pombe* (10, 70) and higher eukaryotes (5), mutations in the *cut1* and *cut2* genes, involved in sister chromatid separation, were recently reported to impair mRNA export in *S. pombe* (4). How these different pathways are connected thus remains to be elucidated.

Mitotic defects of Δ*nup120* mutants are consistent with a mild alteration of the Ran pathway. In *S. pombe*, the multiple Ran-dependent cellular processes are differentially sensitive to the level of active Ran (53). Among these processes, those most sensitive to the level of functional Ran (i.e., microtubule dynamics and chromosome transmission) were also impaired in the Δ*nup120* mutant grown at restrictive temperature. In contrast, phenotypes associated with more severe defects in the Ran pathway (accumulation of septated cells in G_1 with hypercondensed unreplicated chromosomes and a fragmented NE) were not detected in this mutant. Accordingly, the Δ*nup120* mutant behaves in *S. pombe* like strains carrying weak loss-of-function alleles of the Ran pathway.

Gao et al. (23) recently reported that several members of the *S. cerevisiae* Nup84 complex are required for the nuclear accumulation of Ran^{Sc}/Gsp1, a phenotype that could be correlated with an altered association of Ntf2 (the nuclear transport factor of Ran) with the NE. Immunofluorescence analyses

performed in *S. pombe* Δ*nup120* cells suggest that the nuclear accumulation of Spi1 might be slightly diminished at 36°C. Consistently, we also found that expression of nonfunctional Spi1-GFP was specifically toxic in Δ*nup120* and in Δ*nup133b* cells, but not in wild-type or Δ*nup133a* cells. These data suggest that some of the phenotypes of Nup107-120 complex mutants may reflect a disturbance of the Ran GTPase system. Whether an alteration of nuclear import of Ran^{Sp}/Spi1 in these mutant cells is primarily responsible for the subsequent mitotic-spindle and chromosome segregation defects remains to be determined, and further experimentation will be necessary to establish the mechanism by which the Ran^{Sp}/Spi1 pathway and cell cycle progression are affected.

While poly(A)$^+$ RNAs strongly accumulate within the entire nucleus in Δ*nup120* and Δ*nup133b*/*nup107*-GFP mutants, export of most mRNAs appears to be independent of the Ran-GTPase (12, 63). Accordingly, defects in mRNA export occurring in the Nup107-120 complex mutants are likely to be uncoupled from those induced by alterations of the Ran pathway. In contrast, it is tempting to speculate that the clustering defects observed upon alteration of the ScNup84 and SpNup107-120 complex could somehow be linked to the previously reported requirement for Ran in NE and NPC integrity in both *S. pombe* (16, 41) and *S. cerevisiae* (52).

In conclusion, the data presented here provide functional and genetic links between the *S. pombe* Nup107-120 subcomplex and Ran-dependent mitotic processes. In vertebrates, recent studies suggest additional links between the Nup107-160 complex and Ran: this GTPase was shown to regulate interactions between Nup107 and other nucleoporins that may be required for NPC formation (69). In addition, a fraction of mammalian Nup107, Nup133, and Nup85 localizes at kinetochores in mitosis (7, 28), and Ran was recently shown to regulate kinetochore function (3). Whether these independent studies reflect a general function of the Nup107 complex during mitosis in both yeasts and vertebrates remains quite speculative.

ACKNOWLEDGMENTS

We thank U. Fleig (Institut fuer Mikrobiologie, Duesseldorf, Germany), K. Tatebayashi (Institute of Medical Science, University of Tokyo, Tokyo, Japan), T. Toda (Cancer Research UK, London, United Kingdom), M. Yanagida (Kyoto University, Kyoto, Japan), R. Dhar (National Cancer Institute, National Institutes of Health, Bethesda, Md.), and K. Gull (University of Manchester, Manchester, United Kingdom), for generous gifts of strains, plasmids, and antibodies; I. Tratner and G. Baldacci (Institut Curie, Orsay, France) and B. Arcangioli (Institut Pasteur, Paris, France) for strains, advice, and help with FACS analyses; D. Tenza and J. B. Sibarita (Institut Curie, Paris, France) for thin-section electron microscopy and deconvolution microscopy; P. E. Gleizes (LBME, Toulouse, France) for help with 25S rRNA FISH experiments; N. Ong (Baylor College of Medicine, Houston, Tex.) for technical assistance; and the members of the A. Paoletti (Institut Curie, Paris, France) and V. Doye laboratories for discussions and critical reading of the manuscript.

V.D. was funded by the Institut Curie, the Centre National de la Recherche Scientifique, the Association pour la Recherche contre le Cancer, and La Ligue Contre le Cancer (Comité de Paris). S. W. Baï and J. Rouquette were supported by the French Ministry for Research and Technology and La Ligue contre le Cancer, respectively. S.S. and M.U. were funded by the National Institutes of Health (GM49119).

REFERENCES

1. **Aitchison, J. D., G. Blobel, and M. P. Rout.** 1995. Nup120: a yeast nucleoporin required for NPC distribution and mRNA export. J. Cell Biol. **131:** 1659–1675.
2. **Allen, N. P. C., S. S. Patel, L. Huang, R. J. Chalkley, A. Burlingame, M. Lutzmann, E. C. Hurt, and M. Rexach.** 2002. Deciphering networks of protein interactions at the nuclear pore complex. Mol. Cell. Proteomics **1:**930–946.
3. **Arnaoutov, A., and M. Dasso.** 2003. The Ran GTPase regulates kinetochore function. Dev. Cell **5:**99–111.
4. **Azad, A. K., T. Ideue, Y. Ohshima, and T. Tani.** 2003. A mutation in the gene involved in sister chromatid separation causes a defect in nuclear mRNA export in fission yeast. Biochem. Biophys. Res. Commun. **310:**176–181.
5. **Babu, J. R., K. B. Jeganathan, D. J. Baker, X. Wu, N. Kang-Decker, and J. M. Van Deursen.** 2003. Rae1 is an essential mitotic checkpoint regulator that cooperates with Bub3 to prevent chromosome missegregation. J. Cell Biol. **160:**341–353.
6. **Bähler, J., J. Wu, M. S. Longtine, N. G. Shah, A. McKenzie, A. B. Steever, A. Wach, P. Philippsen, and J. R. Pringle.** 1998. Heterologous modules for efficient and versatile PCR-based gene targeting in *Schizosaccharomyces pombe.* Yeast **14:**943–951.
7. **Belgareh, N., G. Rabut, S. W. Bai, M. van Overbeek, J. Beaudouin, N. Daigle, O. V. Zatsepina, F. Pasteau, V. Labas, M. Fromont-Racine, J. Ellenberg, and V. Doye.** 2001. An evolutionarily conserved NPC subcomplex, which redistributes in part to kinetochores in mammalian cells. J. Cell Biol. **154:**1147–1160.
8. **Belgareh, N., C. Snay-Hodge, F. Pasteau, S. Dagher, C. N. Cole, and V. Doye.** 1998. Functional characterization of a Nup159p-containing nuclear pore subcomplex. Mol. Biol. Cell **9:**3475–3492.
9. **Boehmer, T., J. Enninga, S. Dales, G. Blobel, and H. Zhong.** 2003. Depletion of a single nucleoporin, Nup107, prevents the assembly of a subset of nucleoporins into the nuclear pore complex. Proc. Natl. Acad. Sci. USA **100:**981–985.
10. **Brown, J. A., A. Bharathi, A. Ghosh, W. Whalen, E. Fitzgerald, and R. Dhar.** 1995. A mutation in the *Schizosaccharomyces pombe rae1* gene causes defects in poly(A)$^+$ RNA export and in the cytoskeleton. J. Biol. Chem. **270:**7411–7419.
11. **Chen, D., W. M. Toone, J. Mata, R. Lyne, G. Burns, K. Kivinen, A. Brazma, N. Jones, and J. Bahler.** 2003. Global transcriptional responses of fission yeast to environmental stress. Mol. Biol. Cell **14:**214–229.
12. **Clouse, K. N., M. J. Luo, Z. Zhou, and R. Reed.** 2001. A Ran-independent pathway for export of spliced mRNA. Nat. Cell Biol. **3:**97–99.
13. **Cormack, B. P., R. H. Valdivia, and S. Falkow.** 1996. FACS-optimized mutants of the green fluorescent protein (GFP). Gene **173:**33–38.
14. **Cronshaw, J. M., A. N. Krutchinsky, W. Zhang, B. T. Chait, and M. J. Matunis.** 2002. Proteomic analysis of the mammalian nuclear pore complex. J. Cell Biol. **158:**915–927.
15. **Dasso, M.** 2002. The Ran GTPase: theme and variations. Curr. Biol. **12:** R502–R508.
16. **Demeter, J., M. Morphew, and S. Sazer.** 1995. A mutation in the RCC1-related protein pim1 results in nuclear envelope fragmentation in fission yeast. Proc. Natl. Acad. Sci. USA **92:**1436–1440.
17. **Doye, V., R. Wepf, and E. C. Hurt.** 1994. A novel nuclear pore protein Nup133p with distinct roles in poly(A)$^+$ RNA transport and nuclear pore distribution. EMBO J. **13:**6062–6075.
18. **Fleig, U., S. S. Salus, I. Karig, and S. Sazer.** 2000. The fission yeast Ran GTPase is required for microtubule integrity. J. Cell Biol. **151:**1101–1111.
19. **Fontoura, B. M., G. Blobel, and M. J. Matunis.** 1999. A conserved biogenesis pathway for nucleoporins: proteolytic processing of a 186-kilodalton precursor generates Nup98 and the novel nucleoporin, Nup96. J. Cell Biol. **144:** 1097–1112.
20. **Forsburg, S. L.** 1993. Comparison of *Schizosaccharomyces pombe* expression systems. Nucleic Acids Res. **21:**2955–2956.
21. **Forsburg, S. L., and D. A. Sherman.** 1997. General purpose tagging vectors for fission yeast. Gene **191:**191–195.
22. **Galy, V., I. W. Mattaj, and P. Askjaer.** 2003. *C. elegans* nucleoporins Nup93 and Nup205 determine the limit of nuclear pore complex size exclusion in vivo. Mol. Biol. Cell **14:**5104–5115.
23. **Gao, H., N. Sumanaweera, S. M. Bailer, and U. Stochaj.** 2003. Nuclear accumulation of the small GTPase Gsp1p depends on nucleoporins Nup133p, Rat2p/Nup120p, Nup85p, Nic96p and the acetyl-CoA carboxylase Acc1p. J. Biol. Chem. **278:**25331–25340.
24. **Garcia, M. A., N. Koonrugsa, and T. Toda.** 2002. Two kinesin-like Kin I family proteins in fission yeast regulate the establishment of metaphase and the onset of anaphase A. Curr. Biol. **12:**610–621.
25. **Garcia, M. A., L. Vardy, N. Koonrugsa, and T. Toda.** 2001. Fission yeast ch-TOG/XMAP215 homologue Alp14 connects mitotic spindles with the kinetochore and is a component of the Mad2-dependent spindle checkpoint. EMBO J. **20:**3389–3401.
26. **Gleizes, P. E., J. Noaillac-Depeyre, I. Leger-Silvestre, F. Teulieres, J. Y. Dauxois, D. Pommet, M. C. Azum-Gelade, and N. Gas.** 2001. Ultrastructural

localization of rRNA shows defective nuclear export of preribosomes in mutants of the Nup82p complex. J. Cell Biol. **155:**923–936.
27. **Gorsch, L. C., T. C. Dockendorff, and C. N. Cole.** 1995. A conditional allele of the novel repeat-containing yeast nucleoporin RAT7/NUP159 causes both rapid cessation of mRNA export and reversible clustering of nuclear pore complexes. J. Cell Biol. **129:**939–955.
28. **Harel, A., A. V. Orjalo, T. Vincent, A. Lachish-Zalait, S. Vasu, S. Shah, E. Zimmerman, M. Elbaum, and D. J. Forbes.** 2003. Removal of a single pore subcomplex results in vertebrate nuclei devoid of nuclear pores. Mol. Cell **11:**853–864.
29. **He, X., M. H. Jones, M. Winey, and S. Sazer.** 1998. Mph1, a member of the Mps1-like family of dual specificity protein kinases, is required for the spindle checkpoint in *S. pombe*. J. Cell Sci. **111:**1635–1647.
30. **He, X., T. E. Patterson, and S. Sazer.** 1997. The *Schizosaccharomyces pombe* spindle checkpoint protein mad2p blocks anaphase and genetically interacts with the anaphase-promoting complex. Proc. Natl. Acad. Sci. USA **94:**7965–7970.
31. **Hetzer, M., O. J. Gruss, and I. W. Mattaj.** 2002. The Ran GTPase as a marker of chromosome position in spindle formation and nuclear envelope assembly. Nat. Cell Biol. **4:**E177–E184.
32. **Hirano, T., Y. Hiraoka, and M. Yanagida.** 1988. A temperature-sensitive mutation of the *Schizosaccharomyces pombe* gene *nuc2*+ that encodes a nuclear scaffold-like protein blocks spindle elongation in mitotic anaphase. J. Cell Biol. **106:**1171–1183.
33. **Hopper, A. K.** 2001. Role of Ran GTPase in RNA processing and export of RNA from the nucleus to the cytosol: insights from budding yeast, p. 33–52. *In* M. Rush and P. D'Eustachio (ed.), The small GTPase Ran. P. Kluwer Academic Publishers, Boston, Mass.
34. **Hurt, E., S. Hannus, B. Schmelzl, D. Lau, D. Tollervey, and G. Simos.** 1999. A novel in vivo assay reveals inhibition of ribosomal nuclear export in Ran-cycle and nucleoporin mutants. J. Cell Biol. **144:**389–401.
35. **Keryer, G., B. Di Fiore, C. Celati, K. F. Lechtreck, M. Mogensen, A. Delouvee, P. Lavia, M. Bornens, and A. M. Tassin.** 2003. Part of Ran is associated with AKAP450 at the centrosome: involvement in microtubule-organizing activity. Mol. Biol. Cell **14:**4260–4271.
36. **Lee, M. S., M. Henry, and P. A. Silver.** 1996. A protein that shuttles between the nucleus and the cytoplasm is an important mediator of RNA export. Genes Dev. **10:**1233–1246.
37. **Li, O., C. V. Heath, D. C. Amberg, T. C. Dockendorff, C. S. Copeland, M. Snyder, and C. N. Cole.** 1995. Mutation or deletion of the *Saccharomyces cerevisiae* RAT3/NUP133 gene causes temperature-dependent nuclear accumulation of poly(A)$^+$ RNA and constitutive clustering of nuclear pore complexes. Mol. Biol. Cell **6:**401–417.
38. **Lutzmann, M., R. Kunze, A. Buerer, U. Aebi, and E. Hurt.** 2002. Modular self-assembly of a Y-shaped multiprotein complex from seven nucleoporins. EMBO J. **21:**387–397.
39. **Macara, I. G.** 2001. Transport into and out of the nucleus. Microbiol. Mol. Biol. Rev. **65:**570–594.
40. **Matsumoto, T., and D. Beach.** 1991. Premature initiation of mitosis in yeast lacking RCC1 or an interacting GTPase. Cell **66:**347–360.
41. **Matynia, A., K. Dimitrov, U. Mueller, X. He, and S. Sazer.** 1996. Perturbations in the spi1p GTPase cycle of *Schizosaccharomyces pombe* through its GTPase-activating protein and guanine nucleotide exchange factor components result in similar phenotypic consequences. Mol. Cell. Biol. **16:**6352–6362.
42. **Matynia, A., U. Mueller, N. Ong, J. Demeter, A. L. Granger, K. Hinata, and S. Sazer.** 1998. Isolation and characterization of fission yeast sns mutants defective at the mitosis-to-interphase transition. Genetics **148:**1799–1811.
43. **Maundrell, K.** 1993. Thiamine-repressible expression vectors pREP and pRIP for fission yeast. Gene **123:**127–130.
44. **Moreno, S., A. Klar, and P. Nurse.** 1991. Molecular genetic analysis of fission yeast *Schizosaccharomyces pombe.* Methods Enzymol. **194:**795–823.
45. **Murphy, R., J. L. Watkins, and S. R. Wente.** 1996. GLE2, a *Saccharomyces cerevisiae* homologue of the *Schizosaccharomyces pombe* export factor *RAE1*, is required for nuclear pore complex structure and function. Mol. Biol. Cell **7:**1921–1937.
46. **Niwa, O., and M. Yanagida.** 1985. Triploid meiosis and aneuploidy in *Schizosaccharomyces pombe*: an unstable aneuploid disomic for chromosome III. Curr. Genet. **9:**463–470.
47. **Niwa, O., T. Matsumoto, and M. Yanagida.** 1986. Construction of a minichromosome by deletion and its mitotic and meiotic behaviour in fission yeast. Mol. Gen. Genet. **203:**397–405.
48. **Paoletti, A., N. Bordes, R. Haddad, C. L. Schwartz, F. Chang, and M. Bornens.** 2003. Fission yeast cdc31p is a component of the half-bridge and controls SPB duplication. Mol. Biol. Cell **14:**2793–2808.
49. **Paoletti, A., and F. Chang.** 2000. Analysis of mid1p, a protein required for placement of the cell division site, reveals a link between the nucleus and the cell surface in fission yeast. Mol. Biol. Cell **11:**2757–2773.
50. **Pemberton, L. F., M. P. Rout, and G. Blobel.** 1995. Disruption of the nucleoporin gene NUP133 results in clustering of nuclear pore complexes. Proc. Natl. Acad. Sci. USA **92:**1187–1191.
51. **Rout, M. P., J. D. Aitchison, A. Suprapto, K. Hjertaas, Y. Zhao, and B. T. Chait.** 2000. The yeast nuclear pore complex: composition, architecture, and transport mechanism. J. Cell Biol. **148:**635–651.
52. **Ryan, K. J., J. M. McCaffery, and S. R. Wente.** 2003. The Ran GTPase cycle is required for yeast nuclear pore complex assembly. J. Cell Biol. **160:**1041–1053.
53. **Salus, S. S., J. Demeter, and S. Sazer.** 2002. The Ran GTPase system in fission yeast affects microtubules and cytokinesis in cells that are competent for nucleocytoplasmic protein transport. Mol. Cell. Biol. **22:**8491–8505.
54. **Salus, S. S., and S. Sazer.** 2001. The multiple roles of Ran in fission yeast, p. 123–144. *In* M. Rush and P. D'Eustachio (ed.), The small GTPase Ran. P. Kluwer Academic Publishers, Boston, Mass.
55. **Sazer, S., and M. Dasso.** 2000. The ran decathlon: multiple roles of Ran. J. Cell Sci. **113:**1111–1118.
56. **Sazer, S., and P. Nurse.** 1994. A fission yeast RCC1-related protein is required for the mitosis to interphase transition. EMBO J. **13:**606–615.
57. **Shevchenko, A., M. Wilm, O. Vorm, and M. Mann.** 1996. Mass spectrometric sequencing of proteins silver-stained polyacrylamide gels. Anal. Chem. **68:**850–858.
58. **Siniossoglou, S., M. Lutzmann, H. Santos-Rosa, K. Leonard, S. Mueller, U. Aebi, and E. Hurt.** 2000. Structure and assembly of the Nup84p complex. J. Cell Biol. **149:**41–54.
59. **Siniossoglou, S., C. Wimmer, M. Rieger, V. Doye, H. Tekotte, C. Weise, S. Emig, A. Segref, and E. C. Hurt.** 1996. A novel complex of nucleoporins, which includes Sec13p and a Sec13p homolog, is essential for normal nuclear pores. Cell **84:**265–275.
60. **Tanaka, K., J. Petersen, F. MacIver, D. P. Mulvihill, D. M. Glover, and I. M. Hagan.** 2001. The role of Plo1 kinase in mitotic commitment and septation in *Schizosaccharomyces pombe*. EMBO J. **20:**1259–1270.
61. **Tange, Y., A. Hirata, and O. Niwa.** 2002. An evolutionarily conserved fission yeast protein, Ned1, implicated in normal nuclear morphology and chromosome stability, interacts with Dis3, Pim1/RCC1 and an essential nucleoporin. J. Cell Sci. **115:**4375–4385.
62. **Tatebayashi, K., J. Kato, and H. Ikeda.** 1998. Isolation of a *Schizosaccharomyces pombe* rad21ts mutant that is aberrant in chromosome segregation, microtubule function, DNA repair and sensitive to hydroxyurea: possible involvement of Rad21 in ubiquitin-mediated proteolysis. Genetics **148:**49–57.
63. **Tatebayashi, K., T. Tani, and H. Ikeda.** 2001. Fission yeast Mog1p homologue, which interacts with the small GTPase Ran, is required for mitosis-to-interphase transition and poly(A)$^+$ RNA metabolism. Genetics **157:**1513–1522.
64. **Teixeira, M. T., E. Fabre, and B. Dujon.** 1999. Self-catalyzed cleavage of the yeast nucleoporin Nup145p precursor. J. Biol. Chem. **274:**32439–32444.
65. **Teixeira, M. T., S. Siniossoglou, S. Podtelejnikov, J. C. Benichou, M. Mann, B. Dujon, E. Hurt, and E. Fabre.** 1997. Two functionally distinct domains generated by in vivo cleavage of Nup145p: a novel biogenesis pathway for nucleoporins. EMBO J. **16:**5086–5097.
66. **Tran, P. T., L. Marsh, V. Doye, S. Inoué, and F. Chang.** 2001. Mechanism of nuclear positioning in fission yeast based upon microtubule pushing. J. Cell Biol. **153:**397–411.
67. **Vasu, S., S. Shah, A. Orjalo, M. Park, W. H. Fischer, and D. J. Forbes.** 2001. Novel vertebrate nucleoporins Nup133 and Nup160 play a role in mRNA export. J. Cell Biol. **155:**339–354.
68. **Walther, T. C., A. Alves, H. Pickersgill, I. Loiodice, M. Hetzer, V. Galy, B. B. Hulsmann, T. Kocher, M. Wilm, T. Allen, I. W. Mattaj, and V. Doye.** 2003. The conserved Nup107–160 complex is critical for nuclear pore complex assembly. Cell **113:**195–206.
69. **Walther, T. C., P. Askjaer, M. Gentzel, A. Habermann, G. Griffiths, M. Wilm, I. W. Mattaj, and M. Hetzer.** 2003. RanGTP mediates nuclear pore complex assembly. Nature **424:**689–694.
70. **Whalen, W. A., A. Bharathi, D. Danielewicz, and R. Dhar.** 1997. Advancement through mitosis requires rae1 gene function in fission yeast. Yeast **13:**1167–1179.
71. **Whalen, W. A., J. H. Yoon, R. Shen, and R. Dhar.** 1999. Regulation of mRNA export by nutritional status in fission yeast. Genetics **152:**827–838.
72. **Woods, A., T. Sherwin, R. Sasse, T. H. MacRae, A. J. Baines, and K. Gull.** 1989. Definition of individual components within the cytoskeleton of *Trypanosoma brucei* by a library of monoclonal antibodies. J. Cell Sci. **93:**491–500.
73. **Yoon, J. H., W. A. Whalen, A. Bharathi, R. L. Shen, and R. Dhar.** 1997. Npp106p, a *Schizosaccharomyces pombe* nucleoporin similar to *Saccharomyces cerevisiae* Nic96p, functionally interacts with Rae1p in mRNA export. Mol. Cell. Biol. **17:**7047–7060.
74. **Yoshida, M., and S. Sazer.** 2004. Nucleocytoplasmic transport and nuclear envelope integrity in the fission yeast *Schizosaccharomyces pombe.* Methods **33:**226–238.